The effect of Pd(II) chloride complexes anchoring on the formation and properties of Pd/MgAlOx catalysts

Belskaya, O. B.; Zaikovskii, V. I.; Gulyaeva, T. I.; Talsi, V. P.; Trubina, S. V.; Kvashnina, K.; Nizovskii, A. I.; Kalinkin, A. V.; Bukhtiyarov, V. I.; A. Likholobov, V.;

Originally published:

October 2020

Journal of Catalysis 392(2020), 108-118

DOI: https://doi.org/10.1016/j.jcat.2020.09.021

The effect of Pd(II) chloride complexes anchoring on the formation and properties of Pd/MgAlO$_x$ catalysts

Olga B. Belskaya[a]*, Vladimir I. Zaikovskii[b], Tatiana I. Gulyaeva[a], Valentin P. Talsi[a], Svetlana V. Trubina[c], Krystina O. Kvashnina[d], Alexander I. Nizovskii[b], Alexander V. Kalinkin[b], Valerii I. Bukhtiyarov[b], Vladimir A Likholobov[b]

[a] *Center of New Chemical Technologies BIC, Boreskov Institute of Catalysis, 54 Neftezavodskaya Street, 644040 Omsk, Russia*

[b] *Boreskov Institute of Catalysis, 5 Acad. Lavrentieva Ave., 630090 Novosibirsk, Russia*

[c] *Nikolaev Institute of Inorganic Chemistry, 3 Acad. Lavrentieva Ave. 630090, Novosibirsk, Russia*

[d] *ESRF-The European Synchrotron, CS40220, 38043 Grenoble Cedex 9, France*

* Corresponding author: Olga B. Belskaya

E-mail: obelska@ihcp.ru

Phone: +7 (3812) 670 474, Fax: +7 (3812) 646 156

Abstract

Pd(II) chloride complexes were anchored using magnesium-aluminum layered double hydroxides (LDHs) with interlayer anions (CO_3^{2-} and OH^-), which possess different exchange properties, and MgAl mixed oxide during its rehydration. It was shown that the catalysts of the same chemical composition with different size, morphology and electronic state of supported palladium particles can be synthesized by varying the localization of Pd precursor. The properties of Pd/MgAlOx catalysts were studied in aqueous-phase hydrogenation of furfural. Anchoring of the Pd precursor in the interlayer space of LDHs is accompanied by the formation of non-isometric agglomerated palladium particles which contain less oxidized metal and show a higher activity toward hydrogenation of furfural. Magnesium-aluminum oxides in Pd/$MgAlO_x$ catalysts are rehydrated in the aqueous-phase reaction to yield the activated MgAl-LDH species as a support, which promotes the furfural conversion via hydrogenation of the furan cycle.

Key words: palladium catalysts, layered double hydroxides, palladium(II) chloride complexes, palladium particles size and morphology, aqueous-phase furfural hydrogenation

1. Introduction

Supported palladium catalysts, particularly the carbon-supported palladium systems, are classical hydrogenation catalysts [1]. Palladium catalysts of the acid type on oxide supports, including anion-modified ones and zeolites, are intended for certain applications [2]. Base-type palladium catalysts are investigated much more rarely. In this series, noteworthy are the catalysts synthesized using layered double hydroxides (LDHs) of different composition, which demonstrated their advantages in reactions of various types: partial oxidation of methane [3, 4], synthesis of methyl isobutyl ketone from acetone [5, 6], cross-coupling reactions [7, 8], hydrogenation of acetylene to ethylene [9], hydrogenation of phenol to cyclohexanone [10], adsorption and reduction of NO_2 [11], aromatization of n-hexane [12-14], and others.

Owing to their structural features, LDHs have a great potential for deliberate variation of properties of both the support and the deposited metal [15]. Layered double hydroxides of hydrotalcite type with the general formula $[M^{II}_{1-x}M^{III}_{x}(OH)_2]^{x+}[A^{n-}_{x/n}]\ mH_2O$ have the structure consisting of the brucite-like layers and the charge-compensating anions that are located in the interlayer space [16, 17]. After controllable heat treatment, LDHs decompose into mixed oxides $M^{II}(M^{III})O$, which are characterized by high specific surface areas, uniform distribution and interaction between elements [17-20]. Both these materials have attractive properties for their application as the adsorbents and precursors of supports and catalysts [21, 22]. At the same time, it is known [23-26] that the textural and acid-base properties of LDHs and corresponding mixed oxides as well as the structural and electronic properties of a metal in supported catalysts are affected by various factors. The main factors are the chemical composition of LDHs and the method of their synthesis as well as the nature of the active component precursor, method of its anchoring, and conditions of thermal activation.

Palladium is usually introduced by incipient wetness impregnation of an LDH (freshly prepared or precalcined at temperatures in the region of 773 K) with aqueous solutions of its anionic chloride complexes (commonly $[PdCl_4]^{2-}$) without control of the occurring processes [8,

9, 27-30]. Aqueous solutions of $Pd(NO_3)_2$ and $[Pd(NH_3)_4]Cl_2$ are employed more rarely. It is noted that the use of anionic chloride complexes results in the formation of more dispersed palladium particles than the use of cationic (amine or acetate) complexes [31]. Palladium precursors in anhydrous organic solvents are also considered, for example, the solutions of $PdCl_2$ in dimethylformamide [8] or palladium acetylacetonate $[Pd(acac)_2]$ in toluene [11, 32, 33]. In some cases, coprecipitation from aqueous solutions of Mg, Al and Pd nitrate salts is used [11, 30, 33]. Deposition of any precursor is conventionally followed by calcination at temperatures in the region of 573 K and hydrogen reduction of palladium at 523-573 K.

In some studies [33-38], the activity of palladium was investigated in dependence on the features of precursor and the method of synthesis. Thus, in [33], $Pd/Mg(Al)O_x$ catalysts were prepared by three methods: impregnation of the calcined LDH with a toluene solution of $[Pd(acac)_2]$, coprecipitation of solutions of Mg, Pd and Al nitrates at pH 10, and intercalation of preliminarily synthesized Pd-containing negatively charged colloidal particles (Pd-hydroxycitrate) in the interlayer space of LDHs with interlayer nitrate anions ($MgAl\text{-}NO_3$). After a similar pretreatment procedure (calcination at 773 K and reduction at 523 K), the catalysts were tested in the synthesis of 2-methyl-3-phenyl-propanal from benzaldehyde and propanal. Although the sample obtained by impregnation with $[Pd(acac)_2]$ had the highest dispersion of palladium, it showed a low hydrogenation rate. The catalyst synthesized from intercalated precursor demonstrated the maximum activity owing to the optimal adsorption strength of reagents [33].

In [38], Pd/MgAl-LDH catalysts were synthesized via the interaction of aqueous solutions of $Na_2[PdCl_4]$ with MgAl-LDHs having different composition of interlayer anions. The use of $MgAl\text{-}CO_3^{2-}$ led to anchoring of the metal complex on the surface of support, whereas in the case of $MgAl\text{-}NO_3^-$, the anionic complex was introduced by exchanging with the interlayer nitrate anions. The subsequent liquid-phase reduction using $NaBH_4$ resulted in the formation of palladium particles deposited on LDHs and having different sizes and properties depending on

their localization. Thus, the catalyst synthesized by ion exchange contained palladium particles of a smaller size and showed a high selectivity toward the hydrogenation of the C=O bond during the conversion of 2-ethylanthraquinone.

Thus, the analysis of numerous studies revealed that only some works on the synthesis of LDH-based palladium catalysts consider the mechanism of the precursor-support interaction and the role of such interaction in the formation of properties of the supported metal. There are virtually no systematic studies analyzing the transformations of LDHs and a metal complex precursor of palladium during the synthesis of such catalysts. Earlier we have performed detailed studies in this direction for the system MgAl-LDH – Pt(IV) chloride complexes [15]. Studies on the synthesis of supported platinum catalysts demonstrated that the dispersed and electronic states of supported metal and its dehydrogenating activity are affected by both the composition of hydroxide layers (the Mg/Al ratio [15, 39, 40] and the presence of Zn, Ga and Sn as the modifying elements [41-43]) and the nature of interlayer anions in LDHs [44-46]. In the latter case, the use of interlayer anions with different exchange properties made it possible to anchor platinum(IV) anionic chloride complexes both on the surface of hydroxide layers and in the interlayer space. Different features of the metal complex-support interaction produced differences in the composition of metal complex and structure of the support and later provided the formation of supported platinum particles having different morphology and electronic state. Thus, the constricted conditions of the interlayer space led to the formation of platinum particles with the plane morphology, which had an increased electron density owing to the interaction with the basic magnesium-aluminum support, according to XPS data [45, 46].

The objective of the present study was to elucidate regularities in the formation of supported palladium particles in the system MgAl-LDH – $[PdCl_4]^{2-}$. The study was carried out with the Pd(II) chloride complex $H_2[PdCl_4]$. By analogy with $H_2[PtCl_6]$, it is conventionally used for the synthesis of supported catalysts; however, in distinction to Pt(IV) chloride complexes, it is more labile in the ligand exchange and is considerably hydrolyzed both in aqueous solutions

and upon contact with the surface of oxide supports. The synthesis was performed using MgAl-LDHs with the interlayer anions having different anion-exchange properties (CO_3^{2-} and OH^-); in addition, palladium complexes were intercalated in the interlayer space of LDHs also during the rehydration of the mixed oxide in an aqueous solution of $H_2[PdCl_4]$. Transformations of the support and palladium species in different steps of the synthesis and palladium properties in finished catalysts were studied by means of XRD, diffuse reflectance electron spectroscopy, temperature-programmed reduction, electron microscopy, XPS and XAFS. The catalytic properties of the obtained palladium sites were investigated in the model reaction of aqueous-phase hydrogenation of furfural. This reaction is important in the biomass processing scheme. In the logic of this work, it is equally important that it proceeds under mild conditions, excluding sintering of the supported palladium and noticeable deactivation of the catalyst.

2. Experimental

2.1. Catalyst preparation

The synthesis of the MgAl-layered hydroxides having carbonate counter ions was described in detail in [39-47]. The synthesis procedure included coprecipitation of Mg^{2+} and Al^{3+} hydroxides from aqueous solutions (1 mol/L) of nitrate salts upon their interaction with the solutions containing carbonate and hydroxide ions (1 mol/L). The molar ratio of cations Mg^{2+}/Al^{3+} in the salt solution was 2. The synthesis was carried out at pH 10 and a temperature of 333 K. The resulting precipitates of the layered hydroxides with interlayer carbonate anions MgAl-CO_3 were washed and dried at 353 K for 16 h. To obtain samples of activated LDHs, i.e. those containing mostly the interlayer OH anions (MgAl-OH), the initial (MgAl-CO_3) support was calcined at 823 K and hydrated once more in distilled degassed water. The calcination temperature was chosen earlier [45, 48] from thermal analysis data and corresponded to a complete formation of the oxide phase. The hydration of mixed oxide led to restoration of the

LDH layered structure ("memory effect") with appropriate changes in the composition of the interlayer space.

$PdCl_2$ (98%, Aurat, Russia) was dissolved in stoichiometric amount of aqueous HCl to obtain $H_2[PdCl_4]$, which was used as the precursor. Palladium(II) chloride complex was adsorbed from an excess of aqueous solutions (the weight ratio of the support and solution was 1:25) on MgAl-CO_3, MgAl-OH and $MgAlO_x$ (the oxide was obtained by calcining MgAl-CO_3 at 823 K). When the mixed oxide contacted an aqueous solution of the active component precursor, it rehydrated (MgAl-R) with regeneration of the layered hydroxide structure ("memory effect") and simultaneous incorporation of $[PdCl_4]^{2-}$ anions into the interlayer space of the LDH [41]. The chosen methods enabled the complete extraction of the metal complex from the impregnating solutions; the samples designated as $[PdCl_4]$/MgAl-CO_3, $[PdCl_4]$/MgAl-OH and $[PdCl_4]$/MgAl-R and having the palladium content of 1.0 wt.% were obtained.

After calcination at 823 K, the oxide species of palladium and the mixed oxide support phase formed simultaneously. The subsequent treatment in flowing hydrogen at 573 K led to the reduction of palladium. Samples obtained after these steps are designated as PdO/$MgAlO_x$(CO_3, OH, R) and Pd/$MgAlO_x$(CO_3, OH, R), respectively. The contact of the latter with water initiated rehydration of the mixed oxide with restoration of the layered structure of the supports; Pd/$MgAlO_x$(CO_3)-reh, Pd/$MgAlO_x$(OH)-reh and Pd/$MgAlO_x$(R)-reh samples were obtained.

The concentrations of magnesium, aluminum and palladium in the initial solutions and solid samples after their dissolution were determined by inductively coupled plasma atomic emission spectrometry on a Varian 710-ES instrument.

2.2. Characterization

X-ray diffraction (XRD) data on the phase composition of layered hydroxides MgAl-CO_3, MgAl-OH, corresponding oxide phases, and $[PdCl_4]$/MgAl-LDH (before and after heat treatment) were obtained on a D8 Advance (Bruker) diffractometer with monochromatized Cu

K_α radiation at 2θ diffraction angles between 5° and 80°, a scanning step of 0.05°, and a signal accumulation time of 5 s/step.

The diffuse reflectance electron spectroscopy (DRES) of supported complexes was carried out on a UV2501 PC spectrophotometer (Shimadzu) with an ISR240A diffuse reflectance attachment. The spectra were recorded in the 11000–54000 cm^{-1} range with $BaSO_4$ powder as the reference.

The reduction dynamics of the oxidized palladium species supported on mixed oxides $PdO/MgAlO_x(CO_3$, OH, R) was studied by the temperature-programmed reduction (TPR) on an AutoChem-2920 (Micromeritics) chemisorption analyzer. The samples obtained by calcination of LDHs with the anchored palladium complexes in air at 823 K were employed for TPR. TPR was carried out up to 823 K with a 10 K/min heating rate using a 10 vol.%. H_2–Ar gas mixture (the flow rate of 30 mL/min). Palladium dispersion in the reduced samples was estimated by pulse chemisorption of CO probe molecules at room temperature assuming the stoichiometry of [Pd]:[CO] = 1:1 [49].

HAADF-STEM (High Angle Annular Dark Field Scanning Transmission Electron Microscopy) was made with a JEM-2200FS (JEOL) microscope at 200 kV. Suspensions of the catalysts in hexane were deposited on carbon-film-coated copper grids. HAADF-STEM makes it possible to obtain a higher image contrast of Pd particles in comparison with HRTEM. TEM images were recorded on a JEM-2010 (JEOL) electron microscope.

X-ray absorption measurements were performed at the Rossendorf Beamline (ROBL - BM20) of the European Synchrotron Radiation Facility (Grenoble) in transmission mode. The energy of X-ray incident beam was selected using the reflection from a pair of water-cooled Si(111) crystal monochromators. Higher harmonics in the beam were rejected by using two Si mirrors with a Pt coating. The energy calibration was performed using a Pd metal foil sample. XAFS spectra of the samples were measured near the Pd *K* absorption edge in the range of 800 eV above the absorption edge (24350 eV). The quantum flux in recording the spectra was

~ 1×10^{10} photon/s in a beam 200 μm×0.5 mm in size. The local environment of Pd atoms was simulated for unfiltered data with k^2 weighing ($k^2\chi(k)$ Pd *K*) within the wave vector range of Δk = 3–12 $Å^{-1}$ using the EXCURV 98 program [50]. In data processing, the phase and amplitude characteristics were calculated in the von Bart and Hedin approximation. The amplitude suppression S_0^2 due to multielectron processes was determined for a Pd metal foil and then the obtained value (0.9) was set and fixed during simulation of the spectra of the studied samples.

X-ray photoelectron spectra (XPS) were recorded using a SPECS (Germany) spectrometer equipped with several isolated vacuum chambers for fast loading of samples, their thermal treatment and analysis. Samples were transferred between the chambers so as to prevent contacting air. Photoelectron spectra of samples were reproduced in the analyzer chamber at a pressure of $5\cdot10^{-9}$ Torr. For each sample, spectra were recorded using Mg Kα ($h\nu$ = 1253.6 eV) radiation. The binding energy scale of spectrometer was calibrated against the lines of metallic gold and copper, $Au4f_{7/2}$ = 84.0 eV and $Cu2p_{3/2}$ = 932.6 eV. For any radiation, the spectra of non-conducting samples were calibrated against the C1s line whose binding energy was taken equal to 284.8 eV.

Surface acid–base properties of the Pd/$MgAlO_x$(CO_3, OH, R)-reh at the solid–liquid interface were estimated by determining the point of zero charge (PZC) according to the method mentioned in [51, 52]. The samples were placed in aqueous solutions with different initial values of pH. The pH values were measured until the equilibrium was established. Therewith, PZC corresponded to a plateau on the curve of final (equilibrium) pH versus the initial pH. Solutions with the initial pH value ranging from 1 to 13 were prepared with HCl and NaOH. All the measurements were performed using an InLab Easy BNC combined electrode (Mettler Toledo) on a Seven Multi device (Mettler Toledo).

2.3. Catalytic experiment

Liquid-phase hydrogenation of furfural (99%, Sigma–Aldrich) in the presence of synthesized catalysts was examined using a 180 cm^3 steel autoclave. Pretreatment of the catalyst

samples prior to catalytic experiments included calcination in air at 823 K for 3 h and reduction in flowing hydrogen at 573 K for 2 h. A 0.5 g catalyst sample was placed in the autoclave with 40 mL of distilled water. To remove air, an argon flow was passed through the autoclave; after that, the catalyst was pre-reduced with hydrogen at a temperature of 363 K and pressure of 0.5 MPa for 0.5 h under stirring. After the catalyst pre-reduction, 5.0 mL of furfural and 60 mL of distilled water were loaded into the autoclave. Hydrogenation was performed at 363 K and 2.0 MPa hydrogen pressure. The reaction mixture was stirred by a magnetic stirrer at 1400 rpm to prevent external gas-to-liquid diffusion limitations. The reaction was controlled by measuring the volume of consumed hydrogen with a flow mass meter. Additionally, determinations of the composition of intermediate products were carried out (with consumption of 0.05 and 0.1 mol H_2). After completion of the reaction (the absence of hydrogen consumption) and cooling, the aqueous phase was separated from the catalyst by filtering. The products of furfural hydrogenation were identified by ^{1}H NMR, ^{13}C NMR (Bruker Avance-400) and GC–MS (Agilent5973N/6890N). The quantitative determination of the reaction products was carried out by GC (Hewlett Packard 5890 Series II) in a capillary column HP-PONA (50 m × 0.20 mm, Agilent Technologies) with linear heating from 313 to 473 K during the analysis. The ^{1}H and ^{13}C NMR spectra of hydrogenation products were recorded on an Avance 400 (Bruker) NMR spectrometer using D_2O for deuterium stabilization and as the external standard. The pulse programs zg, jmod (APT) with a relaxation delay of 10 s were employed. The lengths of 90° pulses were 3 μs (^{1}H) and 7 μs (^{13}C). The composition of the hydrogenation products was estimated from the integrated intensity of signals from the components in the ^{1}H NMR spectra.

3. Results and Discussion

3.1. The interaction of $H_2[PdCl_4]$ with LDH

The synthesis of MgAl-CO_3 by coprecipitation and the formation of MgAl-OH during rehydration of mixed oxides are well reproducible and provide the specified cationic ratio of

metals [16-22]. Thus, in the performed synthesis, the content of metals in the calcined $MgAlO_x(CO_3)$ was 17.5±0.6 wt.% Al and 31.2 ±0.5 wt.% Mg, which corresponded to the atomic ratio Mg/Al = 2.0 **(Table 1S)**. Structural parameters of these LDHs and corresponding oxides were described in our earlier works [39-46]: X-ray diffraction spectra are characterized by the presence of a series of basal reflections 003 and 006 as well as the peaks of the {0kl} family: 012, 015, 018; {hk0}: 110, and the 113 peak. In the present work, the phase composition of samples was controlled in each step of the synthesis of $Pd/MgAlO_x$ (Mg/Al = 2) catalysts. In the first step, the interaction of $MgAl\text{-}CO_3$, MgAl-OH and $MgAlO_x$ with an aqueous solution of $H_2[PdCl_4]$ (taken for the deposition of 1 wt.% palladium) led to a complete recovery of the metal complex. In the process, the structures of $MgAl\text{-}CO_3$ and MgAl-OH remained virtually unchanged and corresponded to the hydrotalcite structure, PDF 01-089-5434 (**Fig. 1a, b, curves 1**). However, in the case of mixed oxide, its structure was rearranged due to rehydration with the transition to the LDH phase (MgAl-R) (**Fig. 1c, curve 1**). The partial or complete restoration of the layered structure upon contact of mixed oxides with aqueous solutions is the known phenomenon; for example, it was described for solutions of $H_2[PdCl_4]$ and $H_2[PtCl_6]$ metal complexes in [32, 41]. Similar values of parameter *a* (0.305 nm), which are associated with the distances between cations in the brucite-like layers ($a = 2d_{110}$), for $AlMg\text{-}CO_3$, $[PdCl_4]/AlMg\text{-}CO_3$, AlMg-OH, $[PdCl_4$[/AlMg-OH and $[PdCl_4]$/AlMg-R samples and chemical analysis data (**Tables 1S, 2S**) indicate that the cationic composition of hydroxide layers is retained under changes in the composition of the interlayer space of LDH and during its contact with an acidic solution of the Pd precursor. At the same time, parameter *c* ($c = 3d_{003}$), which characterizes the dimensions of the interlayer space and depends on the features, size and concentration of interlayer anions, remained virtually unchanged upon anchoring of $[PdCl_4]^{2-}$ on $MgAl\text{-}CO_3$ and substantially increased (from 2.280 to 2.305 nm) during the synthesis of $[PdCl_4]$/AlMg-OH and $[PdCl_4]$/AlMg-R samples. These structural changes suggest that, for the latter samples, the precursor is fixed in the same way and, possibly, intercalation of hydrated anionic palladium

complexes accompanies both anionic exchange (OH^- for $[PdCl_4]^{2-}$) and rehydration of the mixed oxide.

Earlier we have shown that the difference in localization of the platinum precursor could affect the composition of the anchored complex [15, 45]. The composition of adsorbed complexes is conventionally determined by DRES. The electron spectra of Pd(II) chloride complexes are characterized by two bands: the intense high-frequency band at 45000 cm^{-1} corresponding to the charge transfer from ligand to metal, and a less intense band attributed to the d-d transitions of palladium [53, 54]. The latter is usually used for identification of the hydrolyzed forms of complexes because its position monotonically shifts from 21100 cm^{-1} ($[PdCl_4]^{2-}$) to 26500 cm^{-1} ($[Pd(H_2O)_4]^{2+} \leftrightarrow [Pd(OH)_4]^{2-}$) [54]. The analysis of the obtained electron spectra of adsorbed complexes showed **(Fig. 1S)** that the hydrolyzed forms of complexes are present on all the supports, which is consistent with the high rate of $[PdCl_4]^{2-}$ hydrolysis. The adsorption of $[PdCl_4]^{2-}$ on MgAl-CO_3 is accompanied by the appearance of absorption band at 25000 cm^{-1}, which indicates the occurrence of $[PdCl(H_2O)_3]^+ \leftrightarrow [PdCl(OH)_3]^{2-}$. The anchoring of palladium complexes in the interlayer space with the use of MgAl-OH and MgAl-R leads to the formation of $[Pd(H_2O)_4]^{2+} \leftrightarrow [Pd(OH)_4]^{2-}$ with the absorption band at 26500 cm^{-1}. Depending on the composition of support, differences are observed also in the position of the high-frequency band: for the $[PdCl_4]$/MgAl-CO_3 sample, it substantially shifts toward lower wavenumbers, to 38000 cm^{-1}. The indicated effect is attributed to the coarsening of particles in the complex and the formation of "oxide-like" structures particularly due to binding of metal atoms through the bridging oxygen [55, 56]. In the case of $[PdCl_4]^{2-}$ hydrolysis, the formation of polynuclear palladium hydroxocomplexes is a well-known process [57]; according to DRES data obtained in our study, this process is more pronounced when the hydrolyzed forms of complexes are anchored on the LDH surface.

The EXAFS study of the composition of anchored Pd(II) complexes (**Fig. 2a and Fig. 2Sa**) revealed also that palladium in all the samples is a component of the deeply hydrolyzed

complexes: N(O) is 3.8-4.0, and the coordination number of chlorine does not exceed 0.4 (**Table 1**). As follows from EXAFS data, large particles are not formed on the surface during the hydrolysis – only two coordination spheres can be determined in the environment. When palladium complexes are anchored in the interlayer space, the second sphere (Pd-Pd) is at the detection limit. For the $[PdCl_4]$/MgAl-CO_3 sample, a higher N(Pd) value is observed, which agrees well with the DRES data and may be related to a possible interaction between complexes when the precursor is fixed on the surface with the formation of polynuclear species. The position of the absorption edge and the amplitude of the *A* maximum (the 1s-4p transition) in PdK-XANES spectra suggest that the charge state of palladium atom in all the samples of supported complexes is close to that in PdO oxide (**Fig. 3a**) [58].

It should be noted that the uncoordinated chloride ions formed as a result of the hydrolysis of palladium complexes cannot compete for the position in the interlayer space either with the doubly charged complex anion or with hydroxide ions due to the lower affinity with the hydroxide layers [59].

3.2. High-temperature steps in the synthesis of 1%Pd/MgAlO_x catalysts

The next step in the synthesis of catalysts is high-temperature treatment in the oxidizing medium (calcination in air), which leads to decomposition of the precursor compound and transition of metal to the oxide form. This step is included in the synthesis of various catalysts on oxide supports and commonly results in the formation of more dispersed particles of the supported metal. As follows from the data displayed in **Fig. 1 (curves 2)**, calcination of $[PdCl_4]$/MgAl-LDH at 823 K is accompanied by the formation of mixed magnesium-aluminum oxide with the reflections that are often assigned to the periclase-like structure of the MgO phase with the face-centered cubic lattice [60]; however, in [48] we showed that the structure of this oxide better corresponds to the layered defect spinel (s.g. Fd3m). Note that the lattice parameter *a* (0.418 nm) is similar for all the oxide samples (**Table 2S**), which testifies to their close composition. At the same time, noteworthy is the presence of the stoichiometric magnesium-

aluminum spinel impurity in the sample obtained by calcination of $[PdCl_4]$/MgAl-R; the amount of this impurity does not increase during the further reductive treatment. Previously, it was shown [48] that the formation of spinel occurs upon calcination of LDH, which is characterized by a small size of primary particles and defects. A slight decrease in the intensity and broadening of reflections in the $[PdCl_4]$/MgAl-LDH diffraction pattern (**Fig. 1c, curve 1**) in comparison with Fig. 1a, b, curves 1 suggests that the interaction of the mixed oxide with a palladium acid solution leads to the formation of more dispersed LDH particles. In addition, after calcination of the $[PdCl_4]$/MgAl-CO_3 sample, the peak corresponding to the PdO phase appears in the diffraction pattern **(Fig. 1a**).

The obtained PdO/$MgAlO_x$ samples have a developed texture. Thus, for the PdO/$MgAlO_x(CO_3)$ sample, the specific surface area is 240 $m^2\,g^{-1}$; the total pore volume, 1.1 $cm^3\,g^{-1}$; and the average pore diameter, 18 nm. For the PdO/$MgAlO_x$(OH) sample, these parameters have somewhat lower values, which are equal to 200 $m^2\,g^{-1}$, 0.7 $cm^3\,g^{-1}$ and 12 nm, respectively. The observed texture changes can be caused by a change in the sizes of LDH crystallites, which occurs even during the transition from carbonate, to hydroxide forms of LDH. Thus, the size of crystallites L_a and L_c decreases from 19.8 nm and 13.4 nm for the sample MgAl-CO_3 to 13.2 nm and 8.0 nm for the sample MgAl-OH.

The reductive treatment of PdO/$MgAlO_x$ samples at 573 K did not change the structure of the oxide support (**Fig. 1, curves 3 and Table 2S**). The formation of palladium particles from its oxide species in a hydrogen medium was studied under the TPR conditions. The reduction of palladium commonly occurs at a temperature not higher than 573 K; intense signals reflecting the hydrogen consumption are observed in the TPR profiles obtained at 293-523 K (**Fig. 4**). They correspond to the practically complete reduction of palladium by the reaction $PdO + H_2 \rightarrow Pd + H_2O$ at a molar ratio $n(H_2)/n(Pd^{2+})$ close to one (**Table 2**). The absence of negative peak in the region of 340-350 K, which corresponds to decomposition of palladium β-hydride, indicates the absence of bulky palladium oxides in the samples [28, 29, 53, 57]. The analysis of TPR data

showed that positions of the maxima of consumption peaks depend on the method of palladium precursor introduction. When $H_2[PdCl_4]$ is adsorbed on MgAl-CO_3 and anchored on the external surface, two regions of hydrogen consumption are observed during the reduction of oxide forms of palladium. The quantitative processing of TPR profiles made it possible to establish that only 40% of consumed hydrogen is accounted for the first low-temperature peak (with a maximum of 333 K); more hydrogen (60%) is consumed in the temperature range 370-500 K with a maximum at 423 K. The first peak is similar to that observed during the preparation of Pd/Al_2O_3 catalysts, and it corresponds to the reduction of palladium oxychloride forms adsorbed on the surface of alumina [53]. Based on the data on the chemical composition of the fixed complexes, it can be assumed that high-temperature forms of palladium are obtained from polynuclear palladium hydroxo complexes that interact more strongly with the support surface. According to the EXAFS data, the size of such complexes is small, strong interaction with the support prevents their enlargement during heat treatment, and they are capable of forming highly dispersed particles of supported palladium. Previous studies on the fixation of platinum chloride complexes on the oxide surface [61] give grounds to assume that both of these forms are capable of forming dispersed metal particles on a support, since they have a similar adsorption mechanism on the surface. The fixation of complexes can occur due to the exchange of ligands, i.e. the occurrence of OH groups of the support surface in the coordination sphere of palladium with the corresponding substitution of chloride or hydroxide ligands in the palladium complex.

The reduction of palladium in the samples PdO/MgAlOx obtained from $[PdCl_4]$/MgAl-OH and $[PdCl_4]$/MgAl-R is similar, but different from the sample obtained from $[PdCl_4]$/MgAl-CO_3. This not only demonstrates the influence of the precursor fixation method on the formation of the properties of supported palladium, but also confirms that this method is the same for $[PdCl_4]$/MgAl-OH and $[PdCl_4]$/MgAl-R samples. Hydrogen consumption occurs in a wide temperature range of 320-470 K with a pronounced maximum at 373 K.

Palladium dispersion values in the calcined samples after their reductive treatment, which were measured from CO chemisorption, are relatively low. Nevertheless, in this series (**Table 2**), the $Pd/MgAlO_x(CO_3)$ sample has a higher dispersion. The indicated trend is confirmed by electron microscopy data. According to HAADF-STEM data, palladium particles in the $1\%Pd/MgAlO_x(CO_3)$ sample are smaller and have a more uniform size distribution in comparison with other samples. The average size of palladium particles is 2 nm (**Fig. 5a**). Images of 1%Pd/MgAl(OH) and 1%Pd/MgAl(R) samples are similar to each other but essentially differ from that of $1\%Pd/MgAlO_x(CO_3)$: along with small clusters, there are the agglomerated palladium particles with "dendritic structure" (see, for example, an inset in **Fig. 5b**), both large, up to 100 nm, and smaller ones, ca. 20 nm in size. Many of them have a low contrast (**Fig. 5 b, c**), which may be caused by their "flattened" shape. In this connection, it should be noted that, according to our earlier study [45], anchoring of Pt(IV) chloride complexes in the interlayer space of MgAl-OH is accompanied by the formation of extended platinum particles up to 50 nm in length, which have a small thickness of 0.75 nm, which is close to the size of interlayer space in LDHs (**Fig. 3S**).

Thus, differences in the LDH composition (its anion-exchange properties) and precursor localization affect not only the size but also the morphology of palladium particles. For example, anchoring of $[PdCl_4]^{2-}$ on the $MgAl\text{-}CO_3$ surface after high-temperature treatments results in the formation of spherical palladium particles, which, in spite of their small size, give the diffraction pattern and are detected by XRD (**Fig. 1a**). The driving force in the intercalation of $[PdCl_4]^{2-}$ into the interlayer space is the electrostatic interaction of anionic complexes with positively charged (due to the presence of triply charged aluminum) layers. Based on the nature of LDHs (they are good anion exchangers), this interaction is not very strong. With an increase in temperature and removal of water molecules from the interlayer "galleries", the size of the interlayer space decreases; therefore, the formation of oxide forms of palladium and their enlargement occurs in the constrained conditions of the layered structure. The morphology of the

resulting particles is retained even after the destruction of the LDH structure; their reduction is accompanied by the formation of non-isometric palladium particles, which, according to electron microscopy data, have a larger size (samples 1%Pd/MgAlOx(OH) and 1%Pd/MgAlOx(R)) but do not give reflections in XRD analysis **(Fig. 1 b, c)**. Apparently, it is the non-isometric (plane) morphology that is the reason why we were unable to obtain TEM images of palladium on these samples. At the same time, highly dispersed palladium particles with the size not greater than 2 nm are observed (although not clearly) in TEM images of 1%Pd/$MgAlO_x(CO_3)$ **(Fig. 4S)**.

It is essential that the CO chemisorption method can be used in this study not only to estimate the dispersion of supported palladium but also to reveal its localization. For example, if the step of high-temperature oxidation at 823 K, which destroys the layered structure, is excluded, the reduction of palladium after hydrogen treatment of $[PdCl_4]$/MgAl-(CO_3, OH, R) samples at 573 K proceeds without the destruction of LDHs. Palladium dispersion in the Pd/$MgAlO_x(CO_3)$ sample at different pretreatments (only Red or Ox+Red) was shown to have close values (23 and 29 %, respectively) (**Table 2**). This is an argument in favor of anchoring of the complex on the LDH surface. At the same time, in the Pd/$MgAlO_x$(R) sample, which was synthesized without preliminary destruction of the layers (only Red), palladium is inaccessible to CO chemisorption (D(CO) = 1%), whereas the introduction of the oxidation step (Ox+Red) increases the dispersion up to 19%. These results confirm the assumption about anchoring of the complex in the interlayer space.

The difference in absolute particle sizes of the supported metal, which was found by chemisorption method and electron microscopy method, may be caused by a partial blocking (inaccessibility) of the metal surface and by changes in its adsorption properties with respect to the CO probe molecule. A similar effect was observed in our earlier studies of various approaches to the deposition of platinum complexes on LDHs. The low platinum dispersion revealed by the chemisorption method in the catalyst synthesized with MgAl-OH, at a small size of its particles (according to TEM) and a higher dehydrogenating activity, was attributed to

changes in the adsorption properties of platinum due to the electron density donation from the basic support to the metal [39-42].

The EXAFS study of the reduced samples also demonstrates significant differences in the composition and structure of supported metal depending on the method of precursor anchoring. The reduction leads to the formation of metallic palladium particles with the typical Pd-Pd distance (**Fig. 2b**); however, the Pd-O distance is also observed. It should be noted that the partial oxidation of palladium, especially its small particles, may proceed during the preparation and analysis of samples. This may lead to the appearance of the PdO phase on the diffraction pattern of $Pd/MgAlO_x(CO_3)$ (**Fig. 1a, curve 3**) and create a high coordination number of palladium N(O) in the reduced samples. As follows from **Table 2**, the coordination number of palladium N(Pd) increases in the series of samples $Pd/MgAlO_x(CO_3)$ 0.3 < $Pd/MgAlO_x$(R) 2.1 < $Pd/MgAlO_x$(OH) 4.3; this is consistent with the increase in the particle size of supported palladium, which was revealed by electron microscopy and chemisorption measurements.

The XANES study of palladium catalysts demonstrated (**Fig. 3b**) that 1%$Pd/MgAlO_x$(OH, R) and 1%$Pd/MgAlO_x(CO_3)$ samples actually differ in the state of palladium. In 1%$Pd/MgAlO_x(CO_3)$, palladium has a more oxidized state, which is indicated by shifting of the absorption edge toward higher energies. Changes in the spectrum shape in a more distant energy region (24390 eV, the *B* maximum) also testify to a difference in the ratio between amounts of metallic and oxidized Pd. The increase in intensity of the *B* maximum for 1%$Pd/MgAlO_x$(R) and 1%$Pd/MgAlO_x$(OH) samples is related to a much greater fraction of metallic palladium in them.

These results are in good agreement with the data of the XPS method, which we used to study both the electronic state of supported palladium and the chemical composition of the surface of the prepared catalysts. A typical Pd $3d_{5/2}$ - Pd $3d_{3/2}$ doublet is shown in **Fig. 6.** The position of the signal with the lower BE value (336.1 eV in the $3d_{5/2}$ region) for the sample 1%$Pd/MgAlO_x$(OH) is close to that observed for metallic palladium [62]. For the sample

1%Pd/MgAlOx(CO_3), a pronounced shift of the maximum of the $Pd3d_{5/2}$ band towards higher energies is observed. This value 336.7 eV can be attributed to the electron-deficient palladium species in the oxide form [62, 63]. This BE value can be associated with the higher dispersion of palladium particles in this sample, which is confirmed by the larger atomic ratio Pd/Mg in the series of the studied samples (**Table 2**), and it is in good agreement with the data of chemisorption measurements and electron microscopy. An extremely low concentration of palladium on the surface was obtained with XPS for the sample 1%Pd/MgAl(R), which did not allow us to represent the spectrum correctly, although the position of the signal in the $Pd3d_{5/2}$ region was close to sample 1%Pd/$MgAlO_x$(OH) and also characterized the metallic state of palladium.

According to XPS data, when a chloride complex is used as a palladium precursor, chlorine is present in the finished catalyst (**Table 2**). However, when $H_2[PdCl_4]$ interacts with the MgAl-CO_3 support, the Pd/$MgAlO_x$(CO_3) catalyst contains a smaller amount of chloride ions. In the Pd/MgAlOx(OH, R) samples, the atomic ratio Cl/Mg is close (0.04-0.05) and noticeably exceeds that (0.02) in the Pd/MgAlOx(CO_3) sample. This result also confirms the difference in the mechanisms of the formation of catalysts depending on the composition of the support. It can be assumed that the greater amount of chlorine is due to the fact that it is fixed in the interlayer space after hydrolysis of intercalated chloride complexes and is partially retained after heat treatments.

3.3. Catalytic properties of Pd/$MgAlO_x$ in furfural hydrogenation

The catalysts synthesized in our study were tested also in the aqueous-phase hydrogenation of furfural. This polyfunctional compound is often considered as a convenient object for exploring the possibilities to vary the hydrogenation pathway for obtaining various chemical substances [64, 65]. The pathway of the liquid-phase hydrogenation of furfural strongly depends on the catalyst composition, reaction conditions and features of the solution [65].

Certainly, the use of water as the reaction medium is very attractive. Under mild conditions of the aqueous-phase hydrogenation (< 373 K, < 2 MPa), the main route of transformation is furfural (FAL) → furfuryl alcohol (FOL) → tetrahydrofurfuryl alcohol (THFOL). However, under more severe conditions and in the presence of the catalyst having acid sites, water can be involved in FAL transformations leading to the formation of a broader spectrum of products, particularly those related to the opening of the furan cycle [66, 67]. So it could be expected that the application of the synthesized palladium catalysts containing magnesium-aluminum LDHs without acid sites would make it possible to avoid the reactions with the furan cycle opening and thus to perform the hydrogenation of FAL mostly within the **Scheme 1.**

We estimated the properties of 1%Pd/$MgAlO_x$ catalysts, having different localization of the precursor upon its interaction with LDHs, in the aqueous-phase hydrogenation of furfural. After oxidative (823 K) and reductive (573 K) treatments, the catalysts were contacted with an aqueous solution at 363 K. Under such conditions, the expected structural rearrangement of the support took place. According to XRD data (**Fig. 1, curve 4**), the rehydration was accompanied by restoration of the layered structure of LDHs: all typical reflections are observed in the diffraction patterns; however, in the case of Pd/$MgAlO_x$(R)-reh they are broadened and have a lower intensity, which indicate that the produced material has a more dispersed and defect structure. In addition, the presence of low-intensity peaks of the oxide phase indicates that, under these conditions, the reconstruction was not carried out completely for this sample. Note that, according to [68-70], the rehydration of magnesium-aluminum oxides results in the formation of activated LDHs with OH^- interlayer anions (MgAl-OH), which possess the Brønsted basicity.

The catalytic measurements showed that palladium in the newly synthesized layered material is accessible to reagents. The primary results of the catalytic testing were represented by the time dependences of consumed hydrogen (**Fig. 5S**), which were used to calculate the reaction rates and TOF values (**Table 3**). After 5 hours of the reaction, the complete conversion of furfural was reached on all the samples with the molar ratio of H_2/FAL interaction equal to 2.7-

2.8; the main product was THFOL, and the maximum formation selectivity of the latter (close to 90%) was observed for the 1%Pd/MgAl(OH)-reh sample (**Table 3**). The hydrogenation rate on this sample was only slightly lower than that on 1%Pd/MgAl(CO_3)-reh; however, taking into account considerable differences in palladium dispersion, the 1%Pd/MgAl(OH)-reh catalyst showed the highest TOF value (**Table 3**). The enhancement of the catalytic activity in hydrogenation of furfural with decreasing the dispersion of supported metal was noted earlier [62, 71] and attributed to a lower adsorption strength of the FAL molecule on larger metal particles and to a more energetically favorable cleavage of the H-H bond on them upon activation of the hydrogen molecule. All these properties are inherent in palladium in the metallic unoxidized state, the proportion of which was higher in the 1%Pd/MgAl(OH) catalyst. Additional experiments showed that this catalyst can be used at least twice without loss of activity and after 10 hours of operation no palladium leaching was observed (Fig 9S). The 1%Pd/MgAl(R)-reh sample showed a much lower activity (**Table 3**), probably due to the defect structure of its support (**Fig. 1c, curve 4**) and hence a lower accessibility of palladium sites and, as a consequence, their lower concentration is observed on the support (according to XPS data, **Table 2**).

The composition of the reaction medium was studied at the intermediate steps of hydrogenation corresponding to hydrogen absorption at the H_2/FAL molar ratios equal to 1 and 2. The GC and NMR analysis of the intermediate products of furfural hydrogenation (**Fig. 7 and Fig. 6S)** shows that their composition radically differs from that observed in our earlier study [62], which was performed with Pd/C catalysts under similar reaction conditions (carbon nanotubes (CNTs) and carbon nanoglobules were used as the supports). On Pd/C catalysts, the reaction started from hydrogenation of the carbonyl group, and the fraction of FOL in the reaction mixture reached 80% (the second main product was THFOL) [62]. Therewith, the difference in the dispersion of supported palladium affected the conversion rate but not the composition of products. In the case of catalysts with magnesium-aluminum supports, the

transformation of FAL proceeds mostly by the second pathway i.e via the formation of THFAL **(Figs. 7 and Scheme 1)**, which is present in the aqueous solution as its hydrated form, i.e. hydrogenation of the furan ring in the presence of a more active carbonyl group is observed. The possibility of such hydrogenation pathway may be related to the presence of hydroxyl groups on the surface of support; such groups are strong nucleophiles and interact with the carbonyl group. This reaction may lead to the formation of surface hemiacetals (the appearance of acetal protection of the aldehyde group), which increase the contribution of the furan cycle hydrogenation route. After saturation of the furan cycle, whereas at the furfural conversion above 90% (**Fig. 7),** there occurs a slower (kinetically hindered) step of hydrogenolysis of the C-OH bond in THFAL with the formation of THFOL. Such interpretation was supported by our special experiment, in which the Pd/CNT catalyst (that hydrogenates FAL starting from the aldehyde group) was modified with an alkali (NaOH), and the subsequent hydrogenation of FAL on it led to the formation of a substantial amount of THFAL as a component of the reaction mixture (**Fig. 7S).**

The analysis of **Fig. 7** revealed a difference in the composition of products, namely, in the THFAL/FOL molar ratio, that appeared during hydrogenation of FAL over Pd/MgAlO$_x$(CO$_3$)-reh, 1%Pd/MgAl(OH)-reh and 1%Pd/MgAl(R)-reh catalysts. Thus (for example, with H$_2$/FAL=2), on Pd/MgAlO$_x$(CO$_3$)-reh the THFAL/FOL ratio is equal to 5, whereas in the case of 1%Pd/MgAl(OH)-reh and 1%Pd/MgAl(R)-reh samples this ratio is similar and equal to 2.

This difference confirms the key role of OH groups on the catalyst surface in determining the furfural conversion pathway, because exactly the 1%Pd/MgAlO$_x$(CO$_3$)-reh sample was shown to possess a higher Brønsted basicity. Thus, measurements of the point of zero charge (PZC) on the surface of tested catalysts revealed that pH$_{PZC}$ of Pd/MgAlO$_x$(CO$_3$)-reh is equal to 10.4, which substantially exceeds 9.7 for 1%Pd/MgAl(OH)-reh (**Fig. 8S**). It can be expected that

the lower basicity is associated with the presence of a larger amount of chloride ions in the latter sample.

4. Conclusion

The anchoring of Pd(II) chloride complexes on MgAl-LDH (Mg/Al = 2) has been studied. Variation of the support precursor nature made it possible to fix palladium complexes on the surface (using MgAl-CO_3) and in the interlayer space (using MgAl-OH and during the rehydration of $MgAlO_x$). Palladium is anchored in the hydrolyzed complexes with the possibility to form polynuclear complexes in the case of its location on the LDH surface. Differences in the anchoring of the active component precursor lead (after high-temperature steps of oxidative and reductive treatments) to the formation of catalysts having a similar chemical composition but different sizes and morphology of supported palladium particles. If the carbonate form of LDHs is used, the Pd/$MgAlO_x(CO_3)$ catalyst is characterized by the presence of highly dispersed isometric palladium particles. Anchoring of the Pd precursor in the interlayer space results in the formation of agglomerated palladium particles with “dendritic structure”, which contain a large proportion of palladium in the metallic unoxidized state.

The catalysts in which palladium particles are anchored on the active LDH species possessing the Brønsted basicity are formed upon contact of Pd/$MgAlO_x(CO_3$, OH, R) with water. In the aqueous-phase hydrogenation of furfural, these catalysts provided the complete conversion of FAL; therewith, Pd/$MgAlO_x$(OH)-reh demonstrated a higher activity in the series of tested samples with the THFOL formation selectivity of 87%. The application of magnesium-aluminum LDHs as the supports having Brønsted basicity provided the predominant route of FAL conversion through hydrogenation of the furan ring with the formation of THFAL.

Acknowledgements

The authors are grateful to R.M. Mironenko and L.N. Stepanova for helpful discussions and O.V. Maevskaya, C.V. Vysotsky, A.V. Babenko, R.R. Izmaylov and I.V. Muromtsev for testing the compositions and properties of the synthesized samples.

The research was performed using equipment of the Shared-Use Center "National Center for the Study of Catalysts" at the Boreskov Institute of Catalysis.

The work was carried out in accordance with the State Program of Boreskov Institute of Catalysis (project AAAA-A17-117021450095-1)

References

[1] H.F. Rase, Handbook of Commercial Catalysts: Heterogeneous Catalysts, CRC Press, Boca Raton, 2000, p. 520.

[2] B. Van Vaerenbergh, J. Lauwaert, P. Vermeir, J. De Clercq, J. W. Thybaut, Adv. Catal. 65 (2019) 2.

[3] F. Basile, G. Fornasari, M. Gazzano, A. Vaccari, Appl. Clay Sci. 18 (2001) 51.

[4] F. Basile, G. Fornasari, M. Gazzano, A. Kiennemann, A. Vaccari, J. Catal. 217 (2003) 245.

[5] Y.Z. Chen, C.M. Hwang, C.W. Liaw, Appl. Catal. A 169 (1998) 207.

[6] N. Das, D. Tichit, P. Graffin, B. Coq, Catal. Today 71 (2001) 181.

[7] B. Van Vaerenbergh, Appl. Catal. A 550 (2017) 236.

[8] M.I. Burrueco, M. Mora, C. Jiménez-Sanchidrián, J.R. Ruiz, Appl. Catal. A 485 (2014) 196.

[9] Y. He, J. Fan, J. Feng, C. Luo, P. Yang, D. Li, J. Catal. 331 (2015) 118.

[10] Y.Z. Chen, C.W. Liaw, L.I. Lee, Appl. Catal. A 177 (1999) 1.

[11] B.A. Silletti, R.T. Adams, S.M. Sigmon, A. Nikolopoulos, J.J. Spivey, H.H. Lamb, Catalysis Today 114 (2006) 64.

[12] J. Davis, E.G. Derouane, Nature 349 (1991) 313.

[13] R.J. Davis, E.G. Derouane, J. Catal. 132 (1991) 269.

[14] I.I. Ivanova, A. Paran-Claerbout, M. Seirert, N. Blomend, E.G. Derouane, J. Catal. 158 (1991) 521.

[15] O.B. Belskaya, V.A. Likholobov. Russ. J. Gen. Chem. 90 (2020) 495.

[16] A. Vaccari, Appl. Clay Sci. 14 (1999) 161.

[17] F. Cavani, F. Trifirò, A. Vaccari, Catal. Today 11 (1991) 173.

[18] D. Tichit, S. Ribet, B. Coq, Eur. J. Inorg. Chem. 2 (2001) 539.

[19] V. Rives, S. Kannan, J. Mater. Chem. 10 (2000) 489.

[20] F. Basile, G. Fornasari, M. Gazzano, A. Vaccari, Appl. Clay Sci. 16 (2000) 185.

[21] F. Trifirò, A. Vaccari, in: J.L. Atwood, J.E.D. Davies, D.D. Mac Nicol, F. Vögtle (Eds.), Comprehensive Supramolecular Chemistry, vol. 7, Pergamon Press, Oxford, 1996, p. 251.

[22] D. Tichit, F. Fajula, Stud Surf Sci Catal. 125 (1999) 329.

[23] F. Prinetto, G. Ghiotti, P. Graffin, D. Tichit, Micropor. Mesopor. Mater. 39 (2000) 229.

[24]. F. Prinetto, G. Ghiotti, R. Durand, D. Tichit, J. Phys. Chem. B 104 (2000) 11117.

[25] Z. Gandao, B. Coq, L.C. de Ménorval, D. Tichit, Appl. Catal. A 147 (1996) 395.

[26] V.B. Kazanski, V.Yu. Borovkov, A.I. Serykh, F. Figueras, Catal. Lett. 49 (1997) 35.

[27] J. Zhao, M. Shao, D. Yan, S. Zhang, Z. Lu, Z. Li, X. Cao, B. Wang, M. Wei, D. G. Evans, X. Duan, J. Mater. Chem. A 1 (2013) 5840.

[28] P. Sangeetha, P. Seetharamulu, K. Shanthi, S. Narayanan , K.S. Rama Raob, J. Mol. Catal. A-Chem. 273 (2007) 244.

[29] P. Sangeetha , K. Shanthi, K.S. Rama Rao, B. Viswanathan, P. Selvam, Appl. Catal. A 353 (2009) 160.

[30] S. Narayanan, K. Krishna, Catal. Today 49 (1999) 57.

[31] S. Narayanan, K. Krishna, Appl. Catal. A 174 (1998) 221.

[32] Prinetto, M. Manzoli, G. Ghiotti, M.J.M. Ortiz, D. Tichit, B. Coq, J. Catal. 222 (2004) 238.

[33] D. Tichit, M. de J. M. Ortiz, D. Francova´, C. Ge´rardin, B. Coq, R. Durand, F. Prinetto, G. Ghiotti, Appl. Catal. A 318 (2007) 170.

[34] B. Van Vaerenbergh, Appl. Catal. A 550 (2018) 236.

[35] V. Chikan, A. Molnar, K. Balazsik, J. Catal. 184 (1999) 134.

[36] D. Tichit, R. Durand, P. Graffin, B. Coq, Catal. Lett. 71 (2001) 181.

[37] M.J. Martı´nez-Ortiz, D. Tichit, P. Gonzalez, B. Coq, J. Mol. Catal. A 201 (2003) 199.

[38] C. Miao, T. Hui, Y. Liu, J. Feng, D. Li, J. Catal. 370 (2019) 107.

[39] L.N. Stepanova, O.B. Belskaya, V.A. Likholobov, Kinet. Catal. 58 (2017) 383.

[40] O.B. Belskaya, L.N. Stepanova, T.I. Gulyaeva, D.V. Golinskii, A.S. Belyi, V.A. Likholobov, Kinet. Catal. 56 (2015) 655.

[41] O.B. Belskaya, L.N. Stepanova, A.I. Nizovskii, A.V. Kalinkin, S.B. Erenburg, S.V. Trubina, K.O. Kvashnina, N.N. Leont'eva, T.I. Gulyaeva, M.V. Trenikhin, V.I. Bukhtiyarov, V.A. Likholobov, Catal. Today 329 (2019) 187.

[42] O.B. Belskaya, L.N. Stepanova, T.I. Gulyaeva, S.B. Erenburg, S.V. Trubina, K. O. Kvashnina, A.I. Nizovskii, A.V. Kalinkin, V.I. Zaikovskii, V.I. Bukhtiyarov, V.A. Likholobov, J. Catal. 341 (2016) 13.

[43] O.B. Belskaya, L.N. Stepanova, T.I. Gulyaeva, N.N. Leont′eva, V.I. Zaikovskii, A.N. Salanov, V.A. Likholobov, Kinet. Catal. 57 (2016) 546.

[44] L.N. Stepanova, O.B. Belskaya, M.O. Kazakov, V.A. Likholobov, Kinet. Catal. 54 (2013) 505.

[45] O.B. Belskaya, T.I. Gulyaeva, N.N. Leont′eva, V.I. Zaikovskii, T.V. Larina, T.V. Kireeva, V.P. Doronin, V.A. Likholobov, Kinet. Catal. 52 (2011) 876.

[46] O.B. Belskaya, T.I. Gulyaeva, V.P. Talsi, M.O. Kazakov, A.I. Nizovskii, A.V. Kalinkin, V.I. Bukhtiyarov, V.A. Likholobov, Kinet. Catal. 55 (2014) 786.

[47] O.B. Belskaya, N.N. Leont'eva, T.I. Gulyaeva, S.V. Cherepanova, V.P. Talzi, V.A. Drozdov, V.A. Likholobov, Russ. Chem. Bull. 62 (2013) 2349.

[48] S.V. Cherepanova, N.N. Leont'eva, A.B. Arbuzov, V.A. Drozdov, O.B. Belskaya, N.V. Antonicheva, J. Solid State Chem. 225 (2015) 417.

[49] A. Cabiac, T. Cacciaguerra, P. Trens, R. Durand, G. Delahay, A. Medevielle, D. Plée, B. Coq, Appl. Catal. A 340 (2008) 229.

[50] N. Binsted, EXCURV 98: CCLRC Daresbury Laboratory Computer Program (1998).

[51] J. Park, J.R. Regalbuto, J. Colloid Interface Sci. 175 (1995) 239.

[52] R.M. Mironenko, O.B. Belskaya, V.P. Talsi, T.I. Gulyaeva, M.O. Kazakov, A.I. Nizovskii, A.V. Kalinkin, V.I. Bukhtiyarov, A.V. Lavrenov, V.A. Likholobov, Appl. Catal. A. 469 (2014) 472.

[53] O. B. Belskaya, T. I. Gulyaeva, A. B. Arbuzov, V. K. Duplyakin, and V. A. Likholobov, Kinet. Catal. 51 (2010) 105.

[54] L. Espinosa-Alonso, K. P. de Jong and B. M Weckhuysen, Phys. Chem. Chem. Phys. 12 (2010) 97.

[55] O.B. Belskaya, V.A. Drozdov, T.I. Gulyaeva, A.B. Arbuzov, E.M. Moroz, D.A. Zyuzin, E.A. Paukshtis, T.V. Larina, V.K. Duplyakin, Kinet. Catal. 50 (2009) 880.

[56] B. Tangeysh, M. Fryd, M.A. Ilies, B.B. Wayland, Chem. Commun. 48 (2012) 8955.

[57] O.B. Belskaya, R.M. Mironenko, V.P. Talsi, V.A. Rodionov, T.I. Gulyaeva, S.V. Sysolyatin, V.A. Likholobov, Catal. Today 301 (2018) 258.

[58] Crystallography Open Database 9009820-ID; 1009031-ID; 39852-ID. http://www.crystallography.net/cod/index.php

[59] H.-M. Liu, X.-J. Zhao, Y.-Q. Zhua, H. Yan, Phys. Chem. Chem. Phys. 22 (2020) 2521.

[60] S. Miyata, Clays Clay Miner. 28 (1980) 50.

[61] O.B. Belskaya, R.K. Karymova, D.I. Kochubey, V.K. Duplyakin, Kinet. Catal. 49(5) (2008) 729.

[62] R.M. Mironenko, O.B. Belskaya, T.I. Gulyaeva, A.I. Nizovskii A.V. Kalinkin, V.I. Bukhtiyarov, A.V. Lavrenov, V.A. Likholobov, Catal. Today 249 (2015) 145.

[63] E.A. Monyoncho, S. Ntais, N. Brazeau, J.-J. Wu, C.-L. Sun, E.A. Baranova, ChemElectroChem 3 (2016) 218.

[64] M. López Granados, D.M. Alonso (Ed.), Furfural: An Entry Point of Lignocellulosic in Biorefineries to Produce Renewable Chemicals, Polymers, and Biofuels, World Scientific, Hackensack, 2018, p. 381.

[65] S. Chen, R. Wojcieszak, F. Dumeignil, E. Marceau, and S. Royer, Chem. Rev. 118 (2018) 11023.

[66] R.M. Mironenko, O.B. Belskaya, V.A. Likholobov, Catal. Today in press. DOI: 10.1016/j.cattod.2019.03.023.

[67] R.M. Mironenko, O.B. Belskaya, V.P. Talsi, V.A. Likholobov J. Catal. 389 (2020) 721.

[68] S. Abello´, F. Medina, D. Tichit, J. Pe´rez-Ramı´rez, J.C. Groen, J.E. Sueiras, P. Salagre, Y. Cesteros, Chem. Eur. J. 11 (2005) 728.

[69] M.J. Climent, A. Corma, S. Iborra, A. Velty, J. Mol. Catal. A: Chem. 182/183 (2002) 327.

[70] M.B.J. Roeffaers, B.F. Sels, H. Uji-i, F.C. De Schryver, P.A. Jacobs, D.E. De Vos, J. Hofkens, Nature 439 (2006) 572.

[71] V.V. Pushkarev, N. Musselwhite, K. An, S. Alayoglu, G.A. Somorjai, Nano Lett. 12 (2012) 5196.

Figure captions

Fig. 1. X-ray diffraction patterns of palladium-containing samples synthesized using (a) MgAl-CO_3, (b) MgAl-OH, (c) MgAl-R: (1) [$PdCl_4$]/MgAl-LDH (fixing complex), (2) PdO/$MgAlO_x$ (calcination at 823 K), (3) Pd/$MgAlO_x$ (subsequent reduction at 573 K), (4) Pd/$MgAlO_x$-reh (rehydration of oxide support).

Fig. 2. The moduli of the Fourier transform of experimental PdK-EXAFS spectra (a) supported Pd complexes: (1) [$PdCl_4$]/MgAl-CO_3 (1%Pd), (2) [$PdCl_4$]/MgAl-R (1%Pd), (3) – [$PdCl_4$]/MgAl-OH (1%Pd); (b) supported Pd particles: (1) 1%Pd/$MgAlO_x(CO_3)$, (2) 1%Pd/$MgAlO_x$(R), (3) 1%Pd/$MgAlO_x$(OH).

Fig. 3. Pd K-edge XANES spectra (a) supported Pd complexes: (1) [$PdCl_4$]/MgAl-R (1%Pd), (2) [$PdCl_4$]/MgAl-CO_3 (1%Pd), (3) [$PdCl_4$]/MgAl-OH (1%Pd); (b) supported Pd particles: (1) 1%Pd/$MgAlO_x$(R), (2) 1%Pd/$MgAlO_x(CO_3)$, (3) 1%Pd/$MgAlO_x$(OH).

Fig. 4. TPR profiles of PdO/$MgAlO_x$ (1 wt.% Pd) samples obtained by calcination in air at 823 K: (1) [$PdCl_4$]/MgAl-CO_3, (2) [$PdCl_4$]/MgAl-OH, (3) [PdCl4]/MgAl-R.

Fig. 5. STEM-HAADF images of samples (a) 1%Pd/$MgAlO_x(CO_3)$, (b) 1%Pd/$MgAlO_x$(OH) and (c) 1%Pd/$MgAlO_x$(R).

Fig. 6. Pd 3d XP spectra of (1) 1%Pd/$MgAlO_x(CO_3)$, (2) 1%Pd/$MgAlO_x$(OH). Prior to measurements, the samples were reduced in flowing hydrogen at 573K.

Fig. 7. Furfural conversion (X) and yields (Y) for FOL, THFOL, THFAL vs. the amount of consumed hydrogen during aqueous-phase hydrogenation over $Pd/MgAlO_x(CO_3)$ (a), $Pd/MgAlO_x(OH)$ (b) and $Pd/MgAlO_x(R)$ (c) catalysts at a temperature of 363 K and pressure of 2 MPa.

Table captions

Table 1. Modeling of Pd *K*-edge EXAFS spectra for palladium-containing samples (Pd 1 wt.%): palladium in the complexes supported on LDHs of different composition ([$PdCl_4$]/MgAl-LDH), T(O_2) = 393 K; the reduced palladium supported on magnesium-aluminum mixed oxide obtained from LDHs of different composition (Pd/$MgAlO_x$), T(O_2) = 823 K, T(H_2) = 573 K.

Table 2. Dispersion, particle size of palladium and the ratio of elements on the surface in the reduced catalysts.

Table 3. Catalytic properties of Pd/MgAl-LDH samples in the aqueous-phase hydrogenation of furfural[a].

Scheme captions

Scheme 1. Reaction network for the aqueous-phase hydrogenation of FAL (without opening of the cycle).

Graphical Abstract (for review)

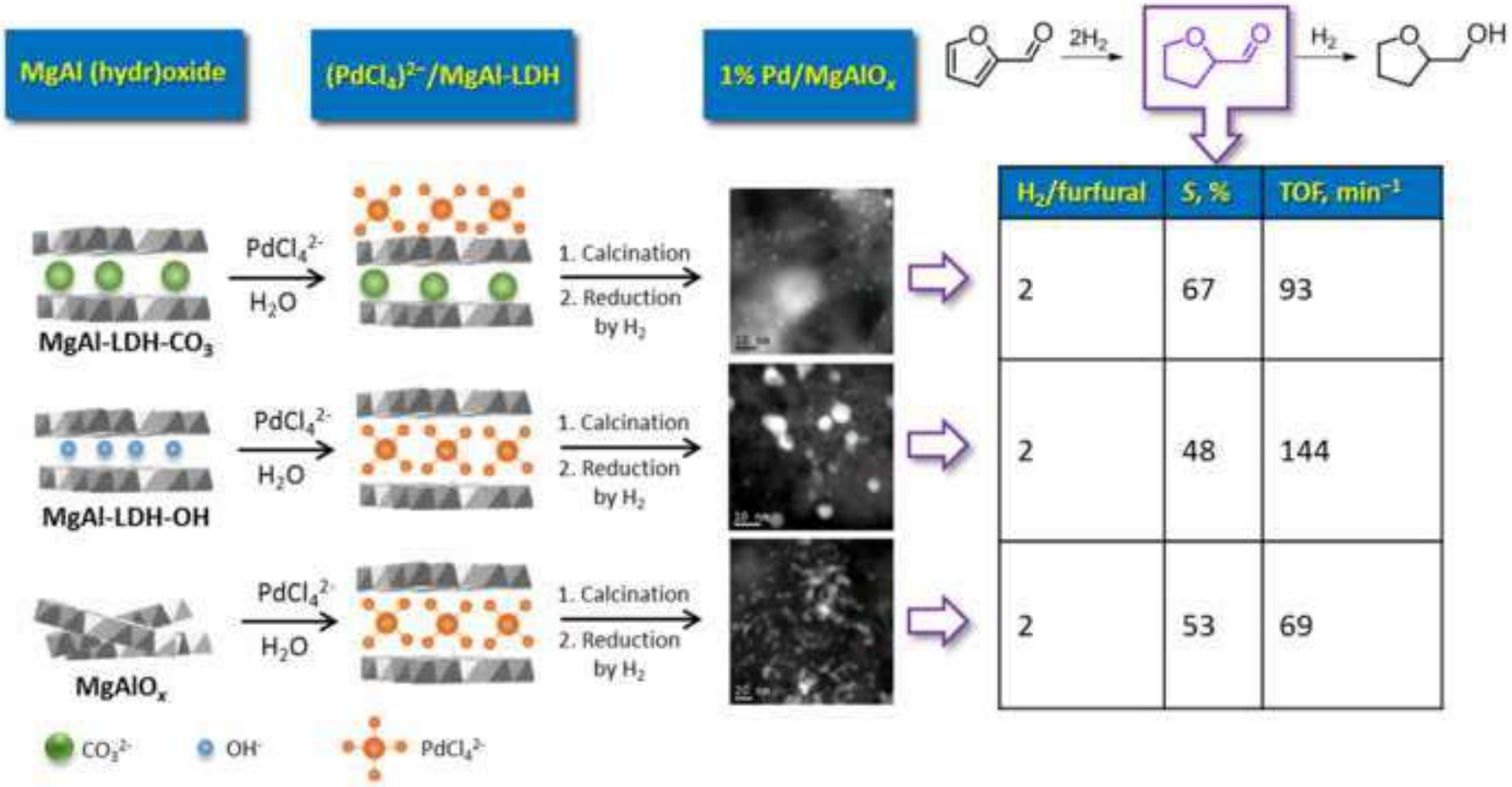

H_2/furfural	S, %	TOF, min^{-1}
2	67	93
2	48	144
2	53	69

Highlights

- Purposeful change of palladium species localization in LDH structure
- Effect of precursor localization on sizes and morphology of supported Pd
- Effect of Pd precursor fixing on palladium activity in aqueous-phase FAL hydrogenation
- Predominant route of FAL conversion through furan ring hydrogenation on Pd/MgAl-LDH

Table

Table 1. Modeling of Pd *K*-edge EXAFS spectra for palladium-containing samples (Pd 1 wt.%): palladium in the complexes supported on LDHs of different composition ([$PdCl_4$]/MgAl-LDH), $T(O_2)$ = 393 K; the reduced palladium supported on magnesium-aluminum mixed oxide obtained from LDHs of different composition (Pd/$MgAlO_x$), $T(O_2)$ = 823 K, $T(H_2)$ = 573 K.

Absorbing atom – backscattering atom	[$PdCl_4$]/MgAl-CO_3		[$PdCl_4$]/MgAl-R		[$PdCl_4$]/MgAl-OH	
	R, Å	N	R, Å	N	R, Å	N
Pd – O	2.02	3.8	2.02	3.9	2.02	4.0
Pd – Pd	3.04	2.2	3.06	1.4	3.05	0.6
	Pd/$MgAlO_x$(CO_3)		Pd/$MgAlO_x$(R)		Pd/$MgAlO_x$(OH)	
	R, Å	N	R, Å	N	R, Å	N
Pd – O	2.02	2.9	2.02	2.5	2.02	2.1
Pd – Pd	2.70	0.3	2.74	2.1	2.74	4.3
Inorganic Crystal Structure Database [58]						
	Pd metal		PdO		K_2PdCl_4	
	R, Å	N	R, Å	N	R, Å	N
Pd – O			2.02	4		
Pd – Pd	2.75	12	3.03	4	4.13	2
Pd – Cl					2.30	4

N – partial coordination numbers, R – interatomic distances, Å. Modeling of EXAFS spectra took into account parameters of the model compounds from the structural database [58]. The measurement accuracy of parameters in the modeling of EXAFS spectra is 0.5 – 1% for interatomic distances and 10% for coordination numbers.

Table 2. Dispersion, particle size of palladium and the ratio of elements on the surface in the reduced catalysts

Sample	n_{H2}/n_{Pd}[a]	D(CO), %	d[c], nm	Atomic ratios[d]	
				Pd:Mg	Cl:Mg
1%Pd/MgAl(CO_3)	0.90	29 (23[b])	3.9	0.039	0.024
1%Pd/MgAl(OH)	0.90	14	8	0.025	0.053
1%Pd/MgAl(R)	1.07	19 (1[b])	5.9	0.007	0.040

[a] Molar ratio obtained from TPR data in the temperature range of 293-523 K
[b] Reduction of the dried [$PdCl_4$]/LDH samples in flowing hydrogen at 573 K without preliminary calcination in air at 823 K
[c] Mean diameter of the particles was calculated from chemisorption data, similar to [57]
[d] Atomic ratios calculated from XPS data

Table 3. Catalytic properties of Pd/MgAl-LDH samples in the aqueous-phase hydrogenation of furfural[a]

Sample	r(H_2)[b] mmol $H_2 \cdot min^{-1}$	TOF[c], mol $H_2 \cdot$mol $Pd_s^{-1} \cdot min^{-1}$	X[d], %	S[d], %		
				THFOL	THFAL	FOL
1%Pd/MgAl(CO_3)	1.28	93	100	72	9	14
1%Pd/MgAl(OH)	0.95	143	100	87	7	2
1%Pd/MgAl(R)	0.62	69	100	84	8	4

[a] Reaction conditions: 95 cm^3 of water, 5.0 cm^3 of furfural, 500 mg of catalyst, T = 363 K, P = 2 MPa.

[b] Reaction rate in (mmoles of H_2) min^{-1} was measured 30 min after the beginning of the reaction at the linear segment of the hydrogen consumption curve, in the range of FAL conversion from 0 to 40%. Preliminary experiments have shown that an aluminum-magnesium support without supported palladium does not catalyze any reactions under the realized conditions.

[c] Turnover frequency (TOF) calculated from the equation TOF = $r(H_2) \cdot n_{Pd}^{-1} \cdot D_{Pd}^{-1}$, where n_{Pd} is the amount of supported palladium (moles), D_{Pd} is the dispersion of palladium determined by pulse chemisorption of CO, and $r(H_2)$ is the rate of hydrogen consumption in (moles of H_2) min^{-1}. The original curves are presented in Fig. 5S.

[d] X is the conversion of furfural according to GC, S is the selectivity of products formation according to GC, and the total content of unidentified products does not exceed 5%.

Figure

Click here to access/download;Figure;Fig. 1 (color).tif

Figure 1 (color)

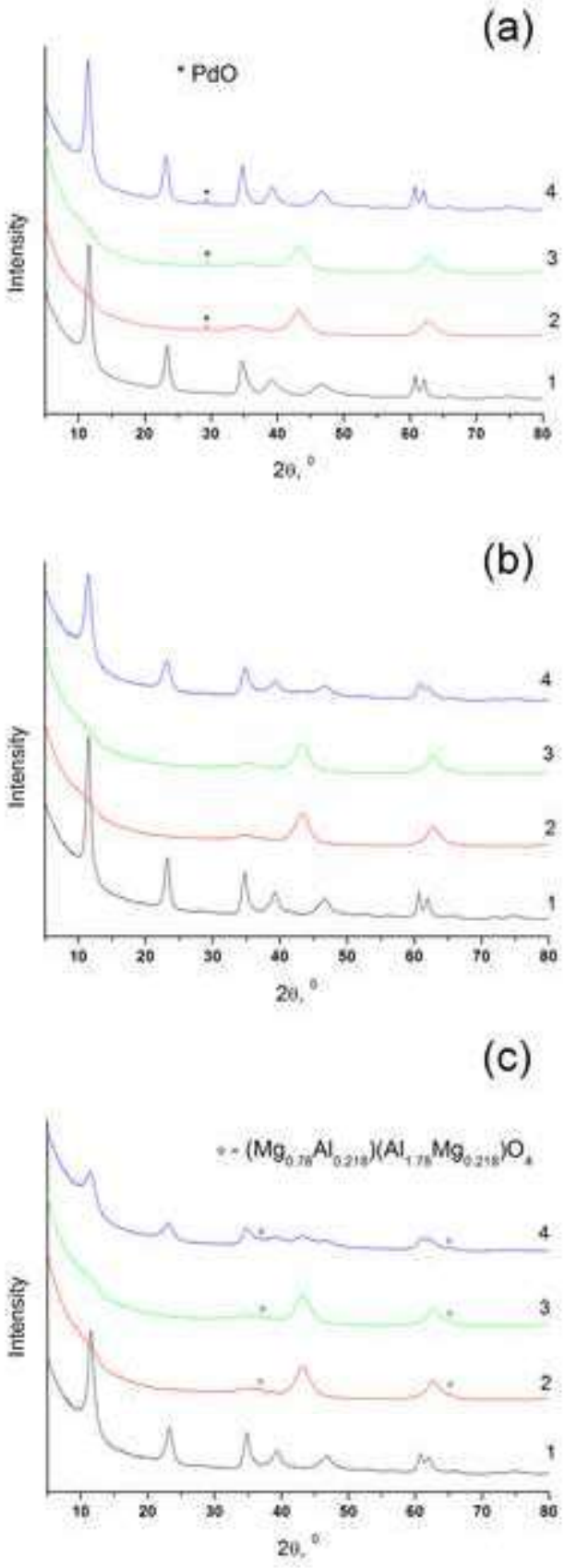

Figure

Click here to access/download;Figure;Fig. 1.tif

Figure 1

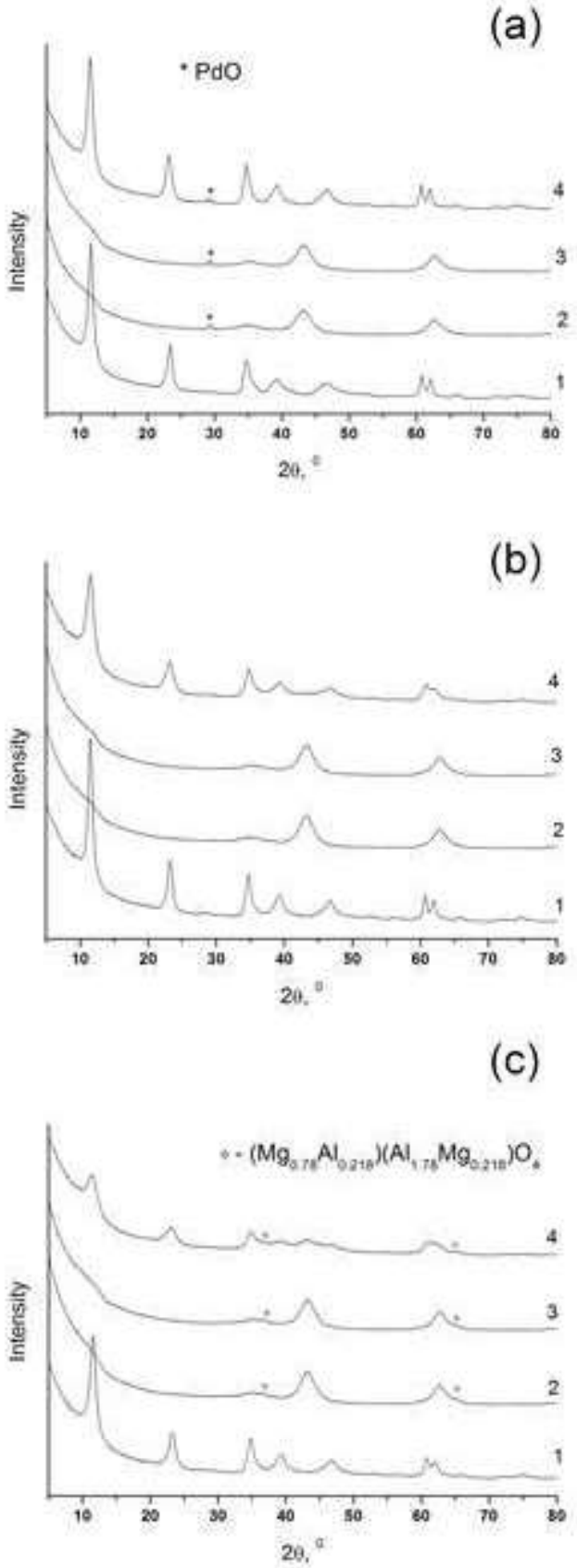

Figure

Click here to access/download;Figure;Fig. 2 (color).tif

Figure 2 (color)

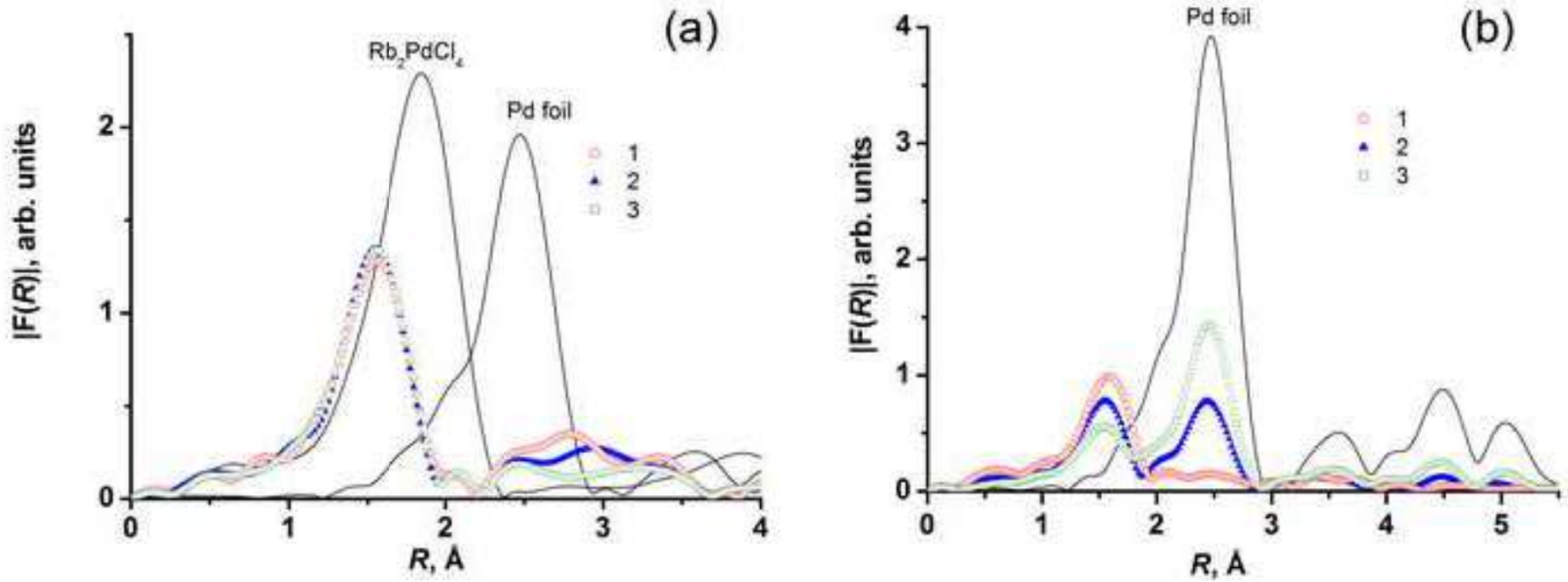

Figure 2

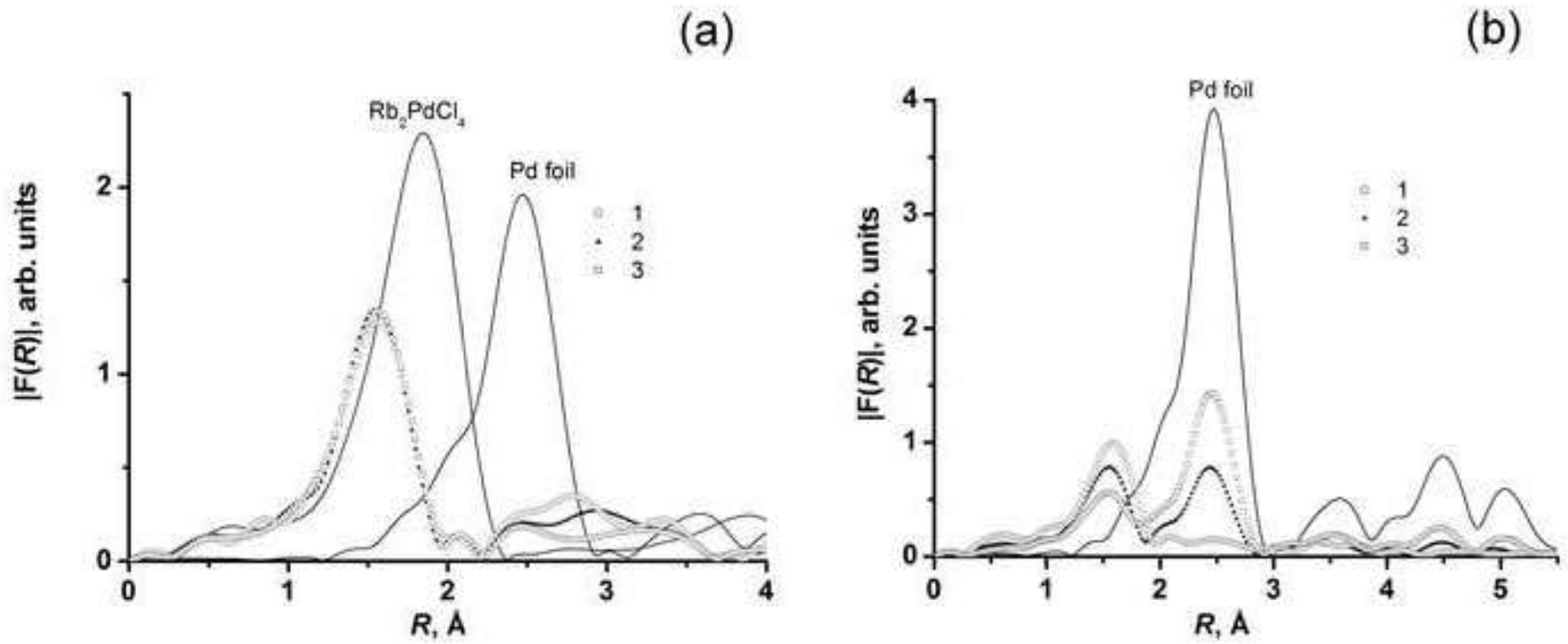

Figure

Click here to access/download;Figure;Fig. 3 (color).tif

Figure 3 (color)

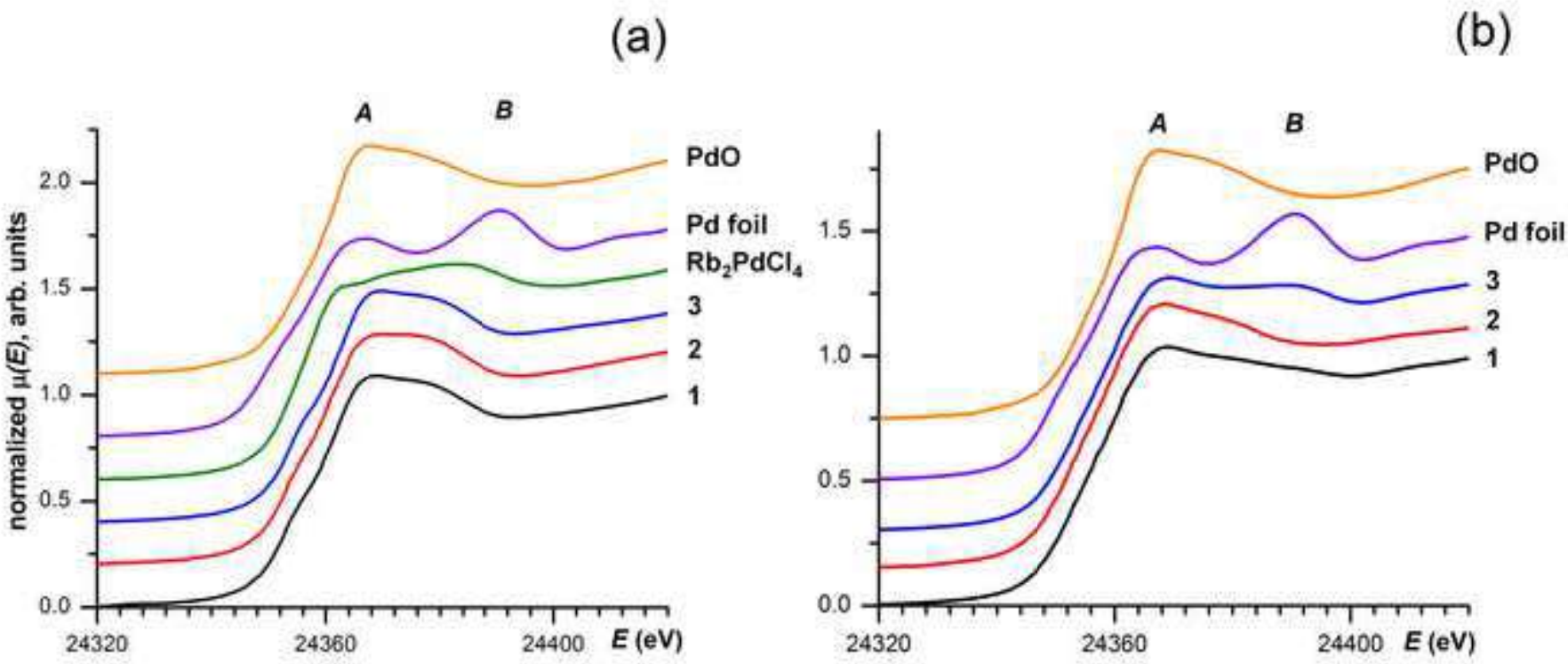

Figure 3

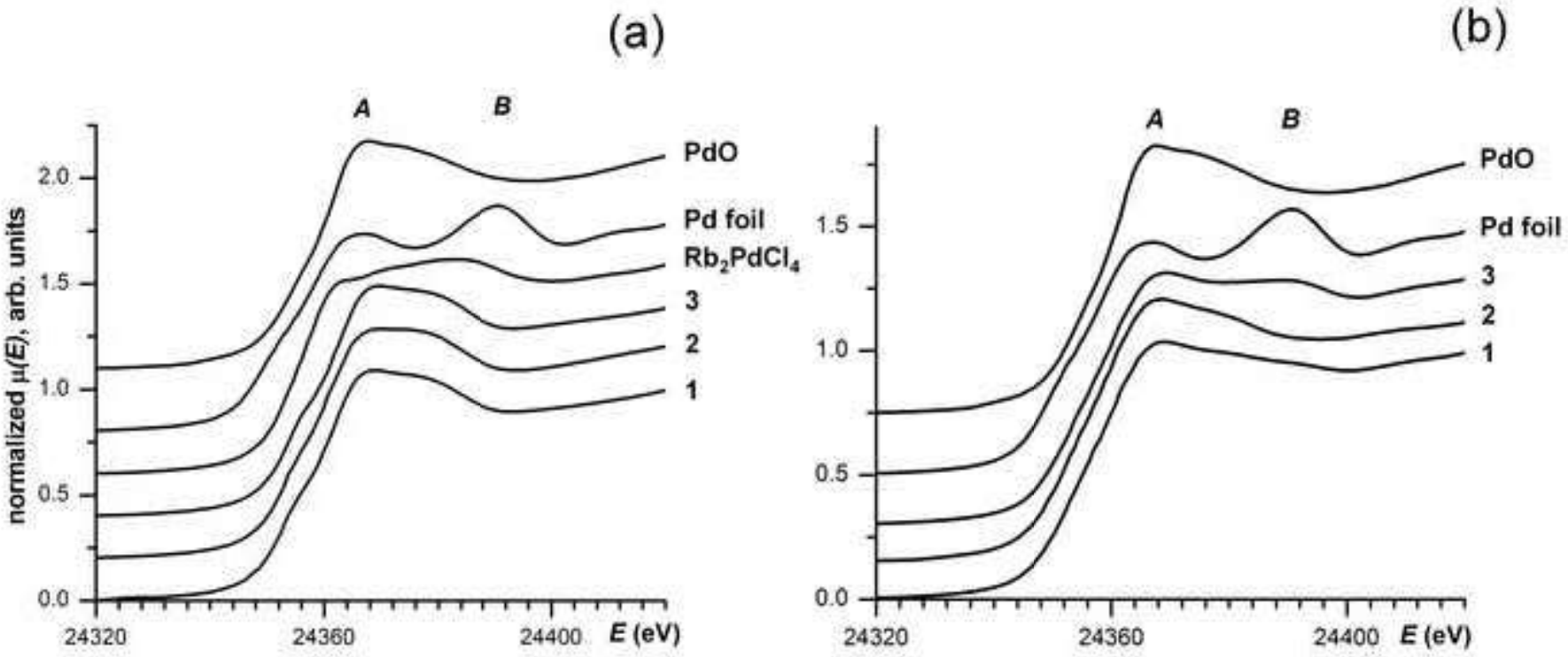

Figure

Click here to access/download;Figure;Fig. 4 (color).tif

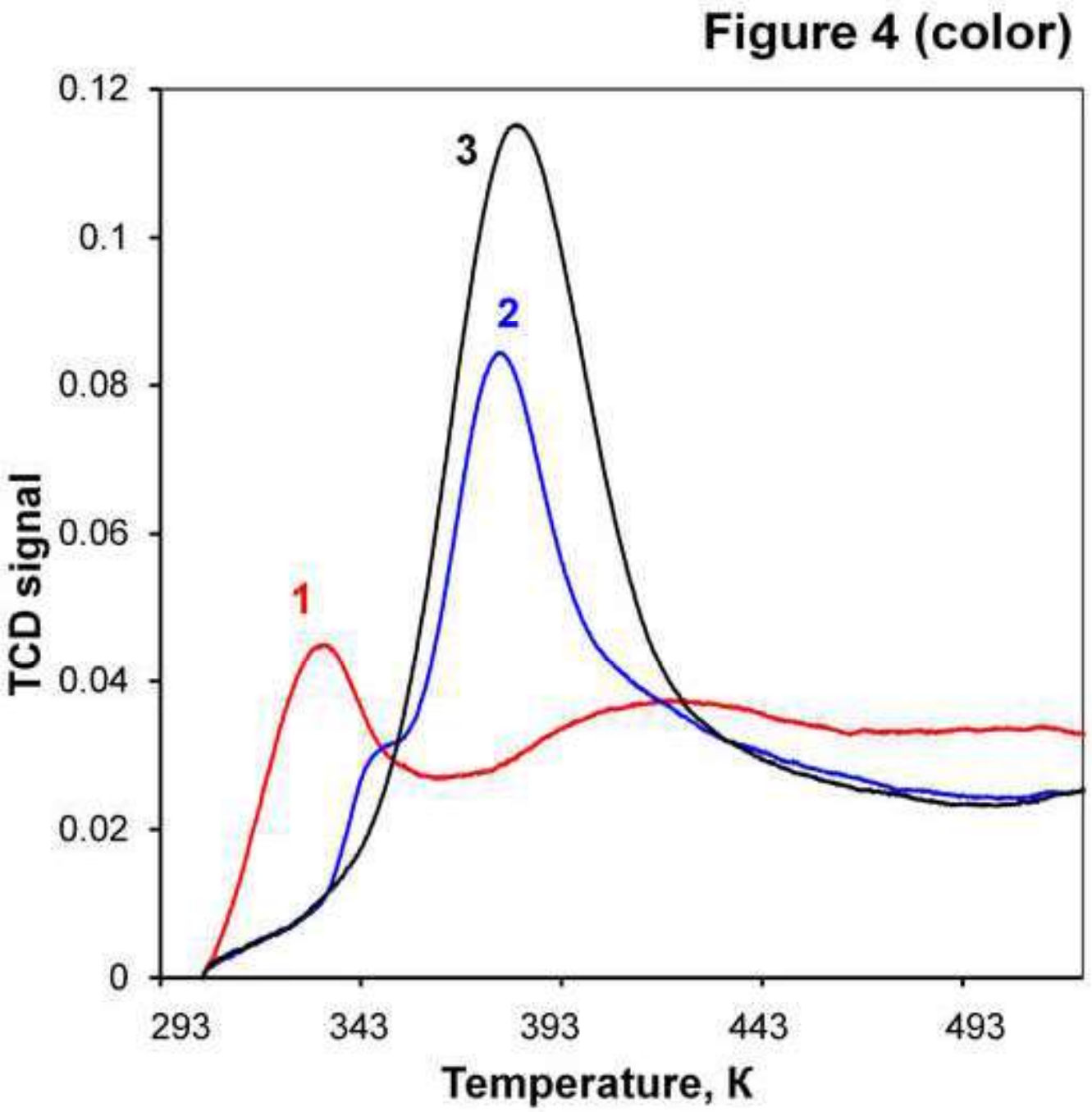

Figure

Click here to access/download;Figure;Fig. 4.tif

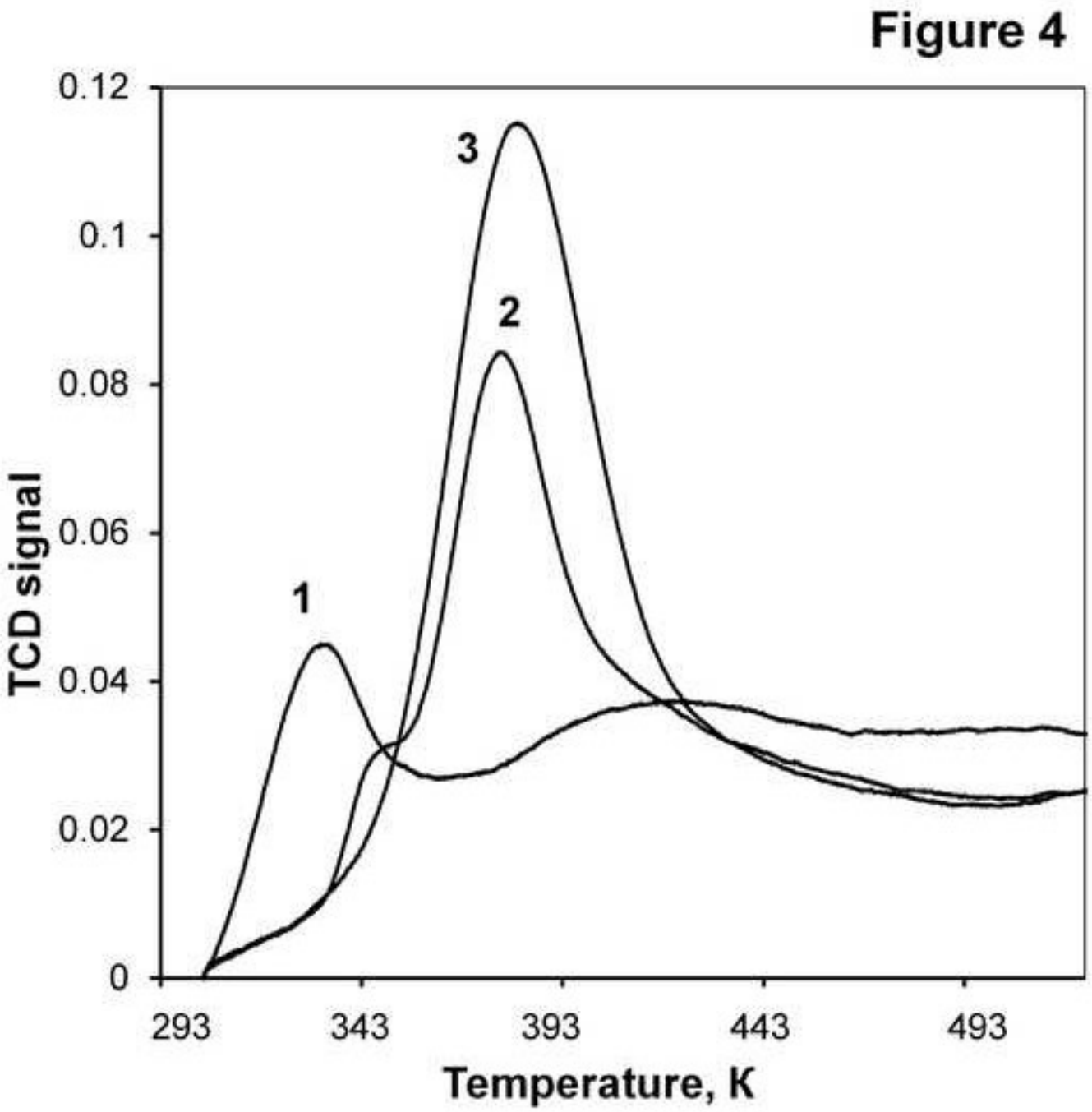

Figure

Click here to access/download;Figure;Fig. 5.tif

Figure 5

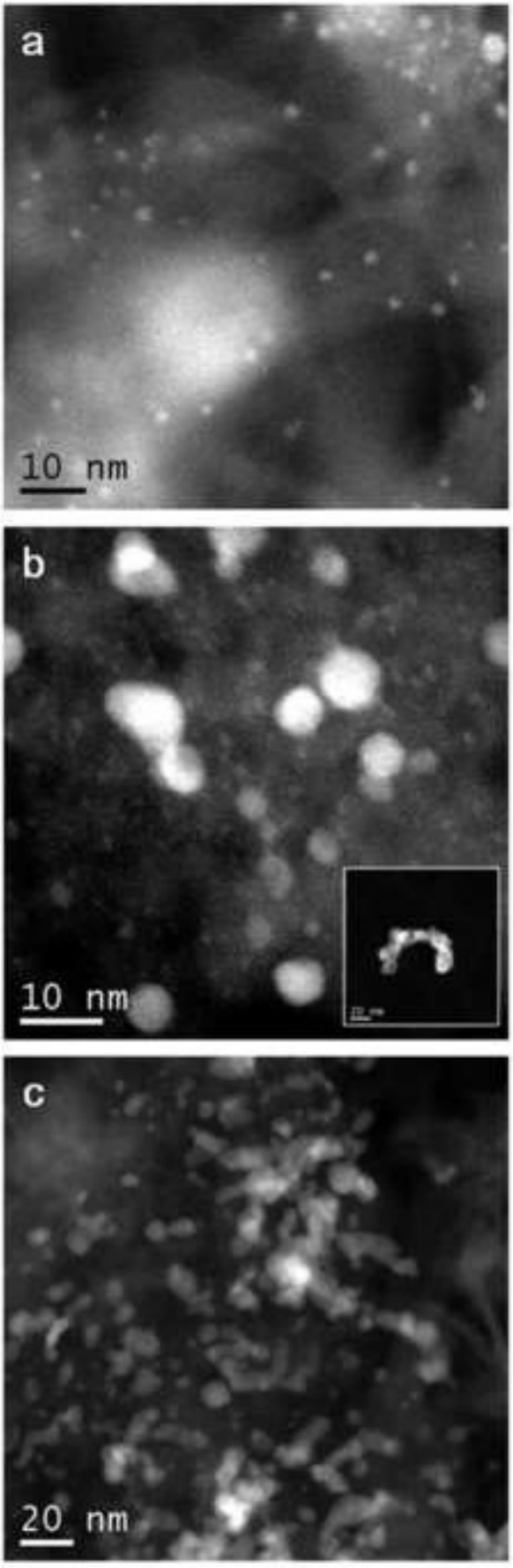

Figure 6

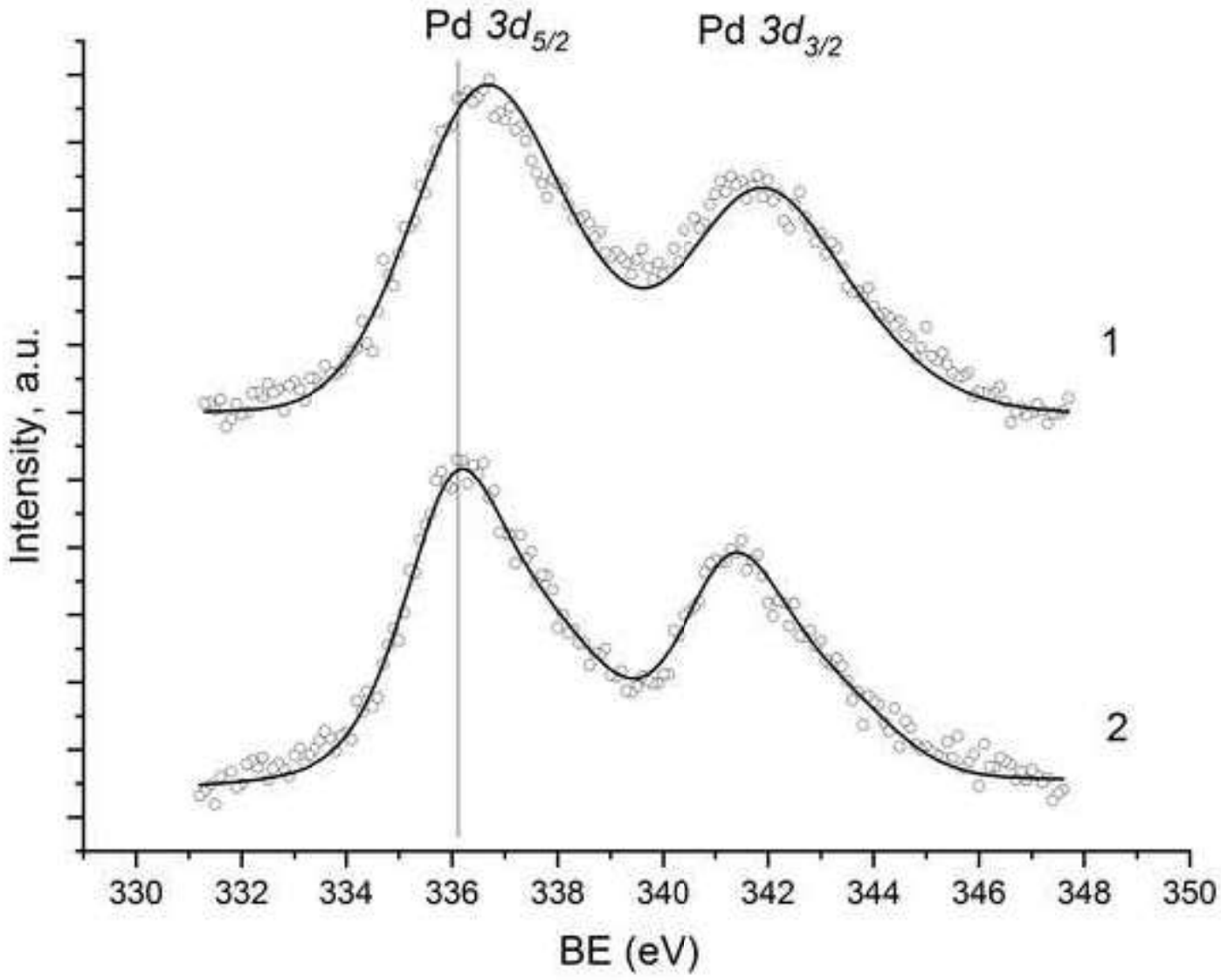

Figure 6 (color)

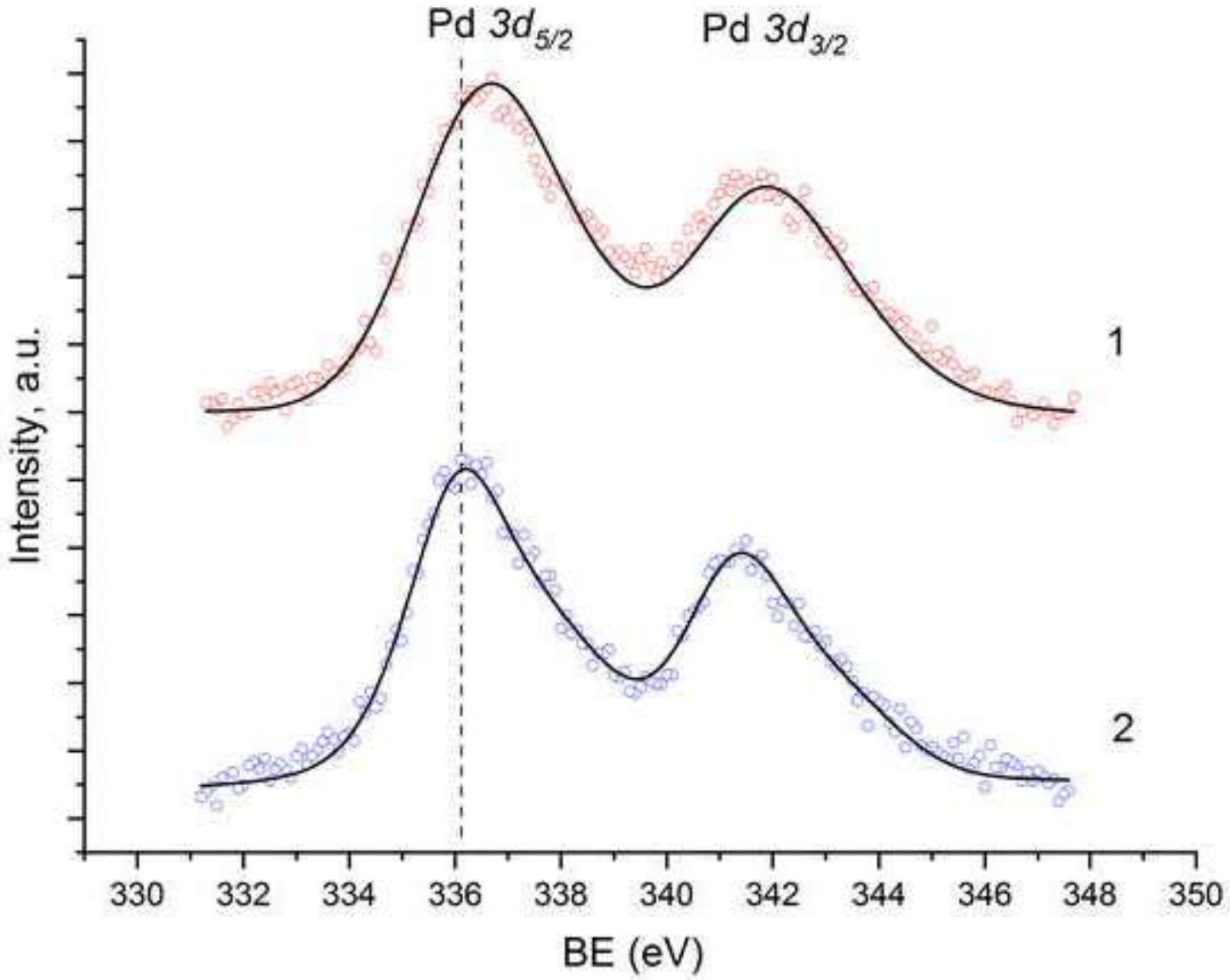

Figure 7

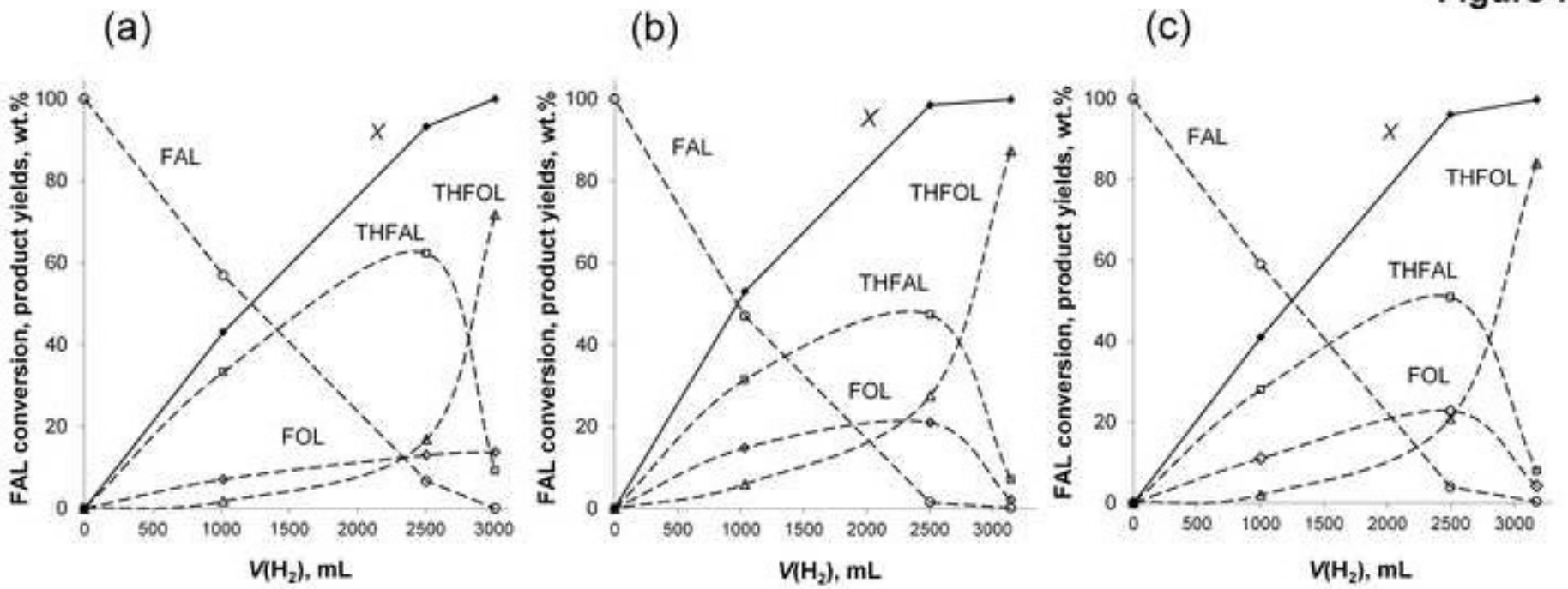

Figure

Click here to access/download;Figure;Fig. 7 (color).tif

Figure 7 (color)